

UNCLASSIFIED

Defense Technical Information Center Compilation Part Notice

ADP010740

TITLE: Measurement Requirements for Improved
Modeling of Arcjet Facility Flows

DISTRIBUTION: Approved for public release, distribution unlimited

This paper is part of the following report:

TITLE: Measurement Techniques for High Enthalpy
and Plasma Flows [Techniques de mesure pour les
écoulements de plasma et les écoulements a haute
enthalpie]

To order the complete compilation report, use: ADA390586

The component part is provided here to allow users access to individually authored sections of proceedings, annals, symposia, ect. However, the component should be considered within the context of the overall compilation report and not as a stand-alone technical report.

The following component part numbers comprise the compilation report:

ADP010736 thru ADP010751

UNCLASSIFIED

Measurement Requirements for Improved Modeling of Arcjet Facility Flows

Presented by
Douglas G. Fletcher
Reacting Flow Environments Branch
NASA Ames Research Center
Moffett Field, CA, 94035-1000

1. Introduction	3A-2
1.1 Historical Development of NASA Ames Arcjet Facilities	3A-2
1.2 Overview of Current NASA Arcjet Facilities	3A-4
1.3 Ames Aerodynamic Heating Facility Arcjet	3A-4
1.4 Arcjet Characterization Using Conventional Instrumentation	3A-5
2. CFD for Arcjet Flows	3A-8
2.1 Motivation for Arcjet Flow Modeling	3A-8
2.2 CFD Requirements for Arcjet Flow Simulations	3A-8
2.3 Strategies for Arcjet Flow Simulations	3A-9
3. Measurement Requirements for Arcjet Flow Modeling	3A-10
3.1 Enthalpy	3A-11
3.2 Arc Heater	3A-11
3.3 Arcjet Nozzle and Free-Stream Flow	3A-12
3.4 Blunt-Body Shock-Layer Flow	3A-12
3.5 Measurement Accuracy Requirements	3A-13
4. Experimental and Computational Investigation of Shock-Layer Flows	3A-14
4.1 Objectives of Investigation	3A-14
4.2 Experimental and Computational Approach	3A-14
4.3 High Pressure Case	3A-16
4.4 Low Pressure Case	3A-20
4.5 Spatially Resolved Measurements	3A-23
4.6 Lessons Learned	3A-23
5. Summary and Recommendations	3A-24
6. Acknowledgements	3A-25
7. References	3A-25

1. Introduction

Current efforts to develop new reusable launch vehicles and to pursue low-cost robotic planetary missions have led to a renewed interest in understanding arcjet flows. Part of this renewed interest is concerned with improving the understanding of arcjet test results and the potential use of available computational-fluid-dynamic (CFD) codes to aid in this effort. These CFD codes have been extensively developed and tested for application to nonequilibrium, hypersonic flow modeling. It is envisioned, perhaps naively, that the application of these CFD codes to the simulation of arcjet flows would serve two purposes: first, the codes would help to characterize the nonequilibrium nature of the arcjet flows; and second, arcjet experiments could potentially be used to validate the flow models. These two objectives are, to some extent, mutually exclusive. However, the purpose of the present discussion is to address what role CFD codes can play in the current arcjet flow characterization effort, and whether or not the simulation of arcjet facility tests can be used to evaluate some of the modeling that is used to formulate these codes.

This presentation is organized into several sections. In the introductory section, the development of large-scale, constricted-arc test facilities within NASA is reviewed, and the current state of flow diagnostics using conventional instrumentation is summarized. The motivation for using CFD to simulate arcjet flows is addressed in the next section, and the basic requirements for CFD models that would be used for these simulations are briefly discussed. This section is followed by a more detailed description of experimental measurements that are needed to initiate credible simulations and to evaluate their fidelity in the different flow regions of an arcjet facility. Observations from a recent combined computational and experimental investigation of shock-layer flows in a large-scale arcjet facility are then used to illustrate the current state of development of diagnostic instrumentation, CFD simulations, and general knowledge in the field of arcjet characterization. Finally, the main points are summarized and recommendations for future efforts are given.

1.1 Development of NASA Ames Arcjet Facilities

Development efforts that led to what we now classify as arcjet test facilities began in the late 1950's with the goal of producing a continuously operable hypersonic ground test facility. This need was driven by both US Department of Defense and NASA mission planning requirements. From the NASA side, planetary missions and the manned space program were pushing aerospace vehicles to higher aerothermodynamic heating rates. Several excellent texts have been written that include a much broader treatment of the his-

torical development of arcjet facilities and plasma arc devices for propulsion.^{1,2} However, for the purpose of introducing the current topic, a brief recapitulation of arcjet facility development activities at NASA Ames Research Center is given below.

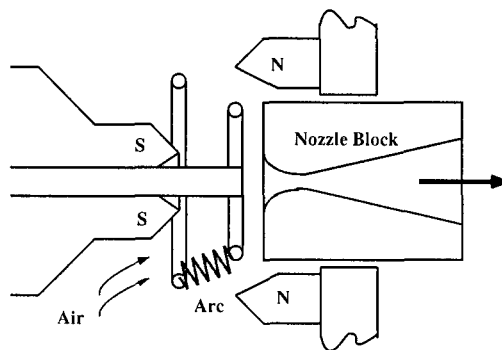


Fig. 1. NASA Ames concentric ring arcjet.

The rather ambitious target capabilities for developing the first Ames arcjet were: 1) 32 MJ/kg enthalpy; 2) 100 atm pressure; 3) 1 MW input power; and 4) continuous and contaminant-free operation. The first successful arcjet that even partially met some of these goals was the Ames Concentric Ring Arcjet,³ which is depicted in Fig. 1. While the device could operate at the intended high pressures, it had a very low efficiency in terms of coupling the electrical energy to the flow. As can be seen in Fig. 1, the arc region is quite small, and most of the incoming air stream bypasses the arc. This resulted in relatively low deposition of energy into the test gas stream.

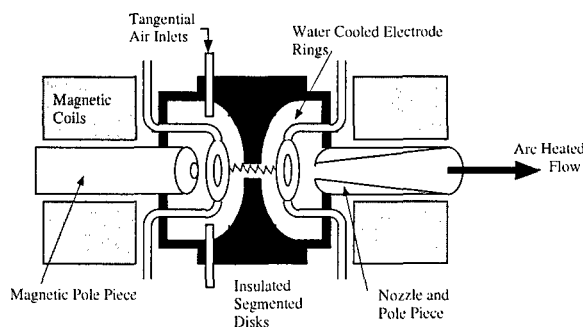


Fig. 2. Early Ames constricted-arc heater.

To improve the coupling of electrical energy into the flow, the next round of heater configurations featured more widely spaced electrodes separated by an orifice plate that is intended to constrict the arc to a relatively small region. It was hoped that forcing the flow and arc through the same small region would improve the electrical energy deposition and raise the stream enthalpy. Figure 2 shows an example of this device, which did show an improvement in energy deposition. However, it proved to be nearly impossible to prevent the arc from attaching at the edge of the orifice plate,

and excessive arc-induced failures produced further design modifications.

Subsequent efforts resulted in the development of supersonic arcjets,⁴ which achieved high enthalpies and low heat loss by extending the arc through the throat region before attachment downstream in the low pressure, expanded flow region. A schematic of one of the earlier versions is shown in Fig. 3. Erosion of the downstream attachment point was minimal for this type of arcjet because of the diffuse nature of the arc at the low pressures of the supersonic flow region. The constrictor diameter was only 6.4 mm, but the heater performance was pretty much as predicted, and there appeared to be a substantial gain in electrical energy deposition. Shortly thereafter a second supersonic arcjet was developed with a 25.4 mm diameter constrictor and this device delivered enthalpies on the order of 900 MJ/kg on the flow centerline.⁵ Unfortunately, the stream was highly nonuniform and the excessive radial gradients limited the application range of this heater.

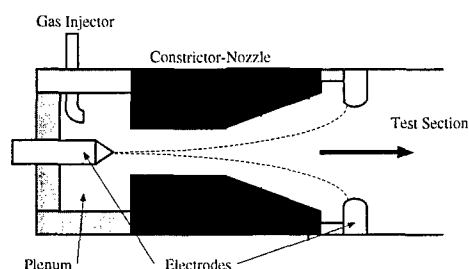


Fig. 3. NASA Ames supersonic, constricted-arc facility.

In one of the more interesting developments that has particular relevance to the current discussion, the ARCFLO code was developed in 1967 to model proposed arc heater configurations.⁶ For the instrumental technology available at the time, comparisons between arcjet performance measurements and ARCFLO predictions were satisfactory. This led to the use of the code in the development of new heater configurations.

Although impressively high enthalpy levels were generated in some of these early devices, there was no great demand for routine operation at those conditions. Instead, the emergence of the shuttle as the primary launch and payload capability for NASA generated a significant demand for test capability in the 20 to 30 MJ/kg range to develop and qualify shuttle-related thermal protection materials. With the exception of meteor ablation studies and work involved with the development of heat shields for planetary-entry missions,⁷ this test condition range has proven satisfactory for a majority of the aerospace community's needs. Progress in providing robust test facilities in the required performance range was enabled by timely improvements in magnetically driven electrode technology.⁸ All of the successful heater designs relied on magnetic fields to spin the arc attachment

point around the electrode to reduce the local heating. However, an optimal combination of geometry, current load, and magnetic field strength leading to extended electrode lifetime could only be found through trial and error, since theoretical models of the combined fluid and plasma dynamics of the electrode were inadequate at that time.

Using the new magnetically driven electrodes, the Ames 20 MW Constricted Arc Jet was built in 1972. A schematic rendering of the constrictor, downstream electrode package and nozzle configuration is shown in Fig. 4. This basic constricted-arc heater configuration has been used continuously, with relatively little variation, in the Ames arcjet facilities since that time. An excellent description of the electrode and constrictor design and performance evaluation is given as part of the report on the Ames 60 MW arcjet,⁹ which is still in use today.

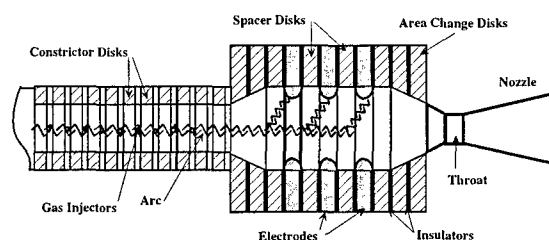


Fig. 4. Current version of Ames constricted-arc heater.

In the late 60's and early 70's arcjets were in use at aerospace companies and research centers around the world. It appeared that arcjets would find extensive use as aerothermodynamic test facilities where fundamental investigations of real gas phenomena could be conducted. Although they did not provide perfect simulation of atmospheric flight environments, arcjets had a significant advantage over impulse facilities in that they could be operated at high enthalpy levels for long periods of time. Unfortunately, it proved to be very difficult to establish just what operating enthalpy level was actually reached. In fact, the inability to characterize the arcjet stream conditions ultimately limited arcjets mainly to applications where complete knowledge of stream conditions was not a requirement for evaluating test results.

In a review of ground-test facility simulations of poorly understood real-gas phenomena, Park¹⁰ identified seven important problems: 1) determining aerodynamic parameters; 2) viscous/shock interactions; 3) boundary layer transition; 4) understanding leeward or base region flows; 5) nonequilibrium radiation; 6) nonequilibrium ionization; and 7) surface catalysis. Park then examined the capabilities of three types of hypersonic ground-test facilities that could be used for fundamental investigations of these problems: 1) impulse facilities (including shock tunnels); 2) ballistic ranges; and 3) arcjets. Arcjets were only deemed suit-

able for studies of nonequilibrium radiation and surface catalysis, and even then adequate specification of the stream conditions was mentioned as a requirement for improving the analysis of test results.¹⁰

Before discussing the issue of stream conditions further, it is useful to examine the current status of large-scale arcjet facilities and their role in thermal protection material test and development. In addition, it is instructive to examine the use of conventional stream characterization instrumentation and how it is used in the interpretation of test measurements.

1.2 Overview of Current NASA Arcjet Facilities

Today, NASA's large-scale arcjet facilities are used mainly to simulate aerothermal heating environments, although there is still some limited use in evaluating supersonic air-breathing propulsion concepts. Our discussions will focus exclusively on facilities, modeling, and measurements that relate to the principal application: aerothermal heating simulation. Two NASA Centers, Johnson and Ames, are currently operating segmented-type constricted-arc heater facilities for this application. This facility is the workhorse for the 20 to 30 MJ/kg enthalpy range of long-duration thermal testing.

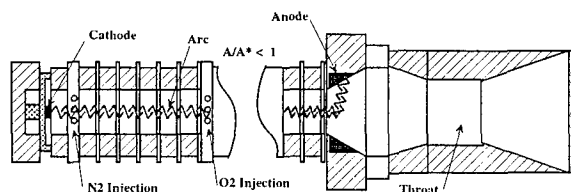


Fig. 5. Current version of JSC TP-1 constricted-arc heater and nozzle.

Arcjet facilities at Johnson Space Center support TPS testing requirements for manned missions. All of the thermal protection materials for shuttle, including tiles, coatings, and fillers, are qualified for use on the basis of tests in these arcjets. Johnson has two 10 MW facilities JSC TP-1, which became operational in 1973, and JSC TP-2, which was upgraded to 10 MW in 1991.¹¹ Both facilities have segmented, constricted-arc heaters. The TP-1 facility is usually arranged with a conical nozzle configuration for stagnation-point testing, while TP-2 is typically configured with a rectangular channel for flat-plate testing. A schematic of the Johnson TP-1 heater and nozzle is presented in Fig. 5, and it shows two noteworthy features. First, because of the tungsten cathode, O₂ is injected separately from N₂ further downstream in the heater to prolong the useful life of the electrode. Although they are injected separately, the two gases are thought to be mixed by the time the downstream electrode package is reached. The second interesting feature is that

the throat diameter is larger than that of the constrictor, which causes some uncertainty regarding the sonic location. Axial velocities in the arc column could actually be quite high, which may inhibit mixing of the O₂ and N₂ streams. The facility is equipped with energy balance instrumentation, which provides a measure of the bulk enthalpy for each test.

The Arcjet Complex at Ames Research Center supports Ames' role as lead NASA Center for thermal protection material development. There are currently three operating segmented, constricted-arc facilities: the Aerodynamic Heating Facility (AHF) and the Panel Test Facility (PTF) are both rated at 20 MW; and the Interactive Heating Facility (IHF) is rated at 60 MW. There are also two operable Huels-type heater facilities, 2x9 Turbulent Flow Facility (TFF) and the Direct Connect Arcjet Facility (DCAF). Two arcjet facility buildings house the different arcjets, which share common steam-ejector vacuum and water-cooling systems. With a shared vacuum system, only one facility can operate at a time. However, facilities can operate sequentially throughout the day with up to 8 runs during a single operating shift. Note that the operating frequency for an arcjet is greater than that of typical large-scale impulse facilities.

A cross section of a typical Ames constricted-arc heater configuration was shown above in Fig. 4. The configuration is different from the JSC TP-1 configuration that was shown in Fig. 5. For the Ames heater, the throat diameter is smaller than the constrictor diameter, so the sonic point will always be located between the converging and diverging sections of the nozzle. Also, both the upstream and downstream electrodes are copper, so oxygen does not need to be injected separately for air tests. Since the overwhelming majority of arcjet tests at Ames Research Center are performed using segmented-type, constricted-arc heaters, Huels-type heaters will not be discussed further.

Even though they are both classified as segmented, constricted-arc heaters, the different designs of the JSC and Ames heaters illustrate the variety of electrodes and nozzles that are in use today. There is no standard design. Consequently, performance will vary widely from facility to facility and characterization of the performance of one facility is by no means applicable to others unless the configuration is exactly duplicated.

1.3 Ames Aerodynamic Heating Facility Arcjet

The Aerodynamic Heating Facility (AHF) Arcjet at NASA Ames Research Center is an example of current large-scale, constricted-arc heater test facilities. A schematic of the facility is shown in Fig. 6. Facility operation is initiated by evacuating the arcjet and then striking an arc in a low-pressure argon stream.¹²

The test gas flow, usually air or nitrogen, is then introduced through the segmented disks along the column, and the arc current is adjusted to achieve the test conditions. Within the arc column, heating by the electrical discharge causes substantial dissociation and ionization of the test gas. The argon start-gas stream is maintained during operation, and additional argon is injected to protect the downstream electrode. Each electrode package is made up of a series of alternating copper rings and spacer disks. The rounded rings are the actual electrodes, and they protrude into the stream to move the arc attachment away from the wall (see Fig. 4). Magnetic windings inside the electrodes rotate the arc attachment point to reduce the heat load on the electrodes. Each electrode can carry up to 500 A of current. Typically, the anode is placed at the upstream end of the arc column to benefit from further cooling by the test gas.

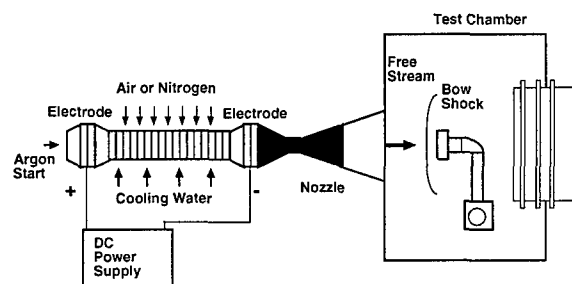


Fig. 6 Schematic of the NASA Ames AHF Arcjet.

Upon leaving the heater, the flow is accelerated to hypersonic speed through a conical, converging-diverging nozzle. During the expansion-driven acceleration, the collision frequency decreases rapidly in the nozzle and the thermochemical state of the flow departs from equilibrium. At some point, the flow chemistry becomes frozen, and this may be followed by freezing of the internal energy distribution of the molecular species. Various nozzle sections can be used to provide expansion ratios ranging from 64 to 576. The flow exits the nozzle and continues expanding into a cabin where material tests are conducted. Material samples are typically inserted into the stream 36 cm downstream of the nozzle exit. Test durations of up to 20 minutes are possible, depending on the particular conditions. During the tests, the stagnation pressure, cabin pressure, and arc heater conditions are continuously monitored.

In a typical test cycle, a preliminary analysis of the expected heat load in a flight application has been performed and a candidate thermal protection material has been selected for testing in an arcjet flow. The test conditions are chosen to attempt to match the expected heat flux for a particular point on a predicted trajectory, such as the peak heating point. Conventional instruments, which will be discussed below, are used to verify the test conditions. The test results

are then interpreted without the benefit of full knowledge of the stream conditions. Currently, relating test results from the arcjets to the intended flight application is more of an art than a science, because the arcjet stream conditions are not sufficiently characterized.

1.4 Arcjet Characterization Using Conventional Instrumentation

The words "Arcjet Characterization" are typically understood to mean specifying the state of the arcjet test stream, and they are referred to throughout this discussion in that context. Although it is important in flow modeling, the need for arcjet characterization is driven primarily by the needs of thermal protection material developers, who need better specification of the stream conditions to relate the results to flight environments. In addition, an improved understanding of arcjet stream conditions in general may also make arcjets more suitable for fundamental studies of real gas phenomena.

The state of arcjet stream characterization in the early 90's was summarized in an excellent and thoughtful review article by Scott.¹³ Both established and novel instrumental techniques were critically reviewed in the article. The article focused mainly on how various diagnostic techniques could be used to characterize the most important stream variables: enthalpy and the degree of nonequilibrium in the stream. Rather than repeat this review, some of the more widely used conventional diagnostics are reviewed briefly below. The limitations of these measurement techniques are discussed to provide background for considering what measurements are required to improve arcjet flow modeling. Newer, less widely used spectroscopic techniques, such as multiphoton spectroscopy will be mentioned later, and are discussed more fully in the second article.

Traditional instruments that are used to obtain flow property measurements include pitot probes and calorimeters. Additional instruments, such as thermocouples and flow meters are used to measure coolant flow rates and temperature rise to perform an energy balance on the facility. Stream surveys are usually performed with a traversing, sting-mounted probe, since the facility can operate continuously and at a level where the instrument can give an equilibrated response to the quantity being measured.

Pitot measurements yield the stagnation pressure behind a shock wave that is generated by the probe. For much of the operating range of today's large-scale arcjet facilities, the pitot, or impact, pressure can be related to the dynamic pressure of the flow, $\rho v^2/2$, through the Rayleigh supersonic pitot relation¹⁴,

$$p_p = \frac{\rho v^2}{\gamma} \left(\frac{2\gamma}{\gamma+1} \right)^{\frac{\gamma-1}{\gamma-1}} \left(\frac{\gamma+1}{2} \right)^{\frac{\gamma}{\gamma-1}}, \text{ for } M \gg 1. \quad (1)$$

In the above expression, γ is the ratio of specific heats for the gas, M is the Mach number, p_p is the pitot pressure, ρ is the stream density, and v is the velocity. Although ρ and v are both important stream variables for arcjet flow characterization, a determination of each variable cannot be made without an additional measurement. For typical facility operating conditions the flow velocity is a considerably larger quantity than the stream density, so a strategy for determining both variables should involve a velocity measurement.

Energy Balance - Most arcjet facilities are equipped with instruments that can be used to perform an energy balance on the arcjet facility as a whole. Owing to its simplicity, the energy balance approach remains by far the most commonly used for characterizing the arcjet stream. The basic principle of the measurement is illustrated in Fig. 7, which shows the arc-jet operation measurements that must be acquired to perform the energy balance. A simple first law relationship is invoked for the system,

$$\dot{m} h_{\text{avg}} = VI - \dot{m} c_p (\Delta T_{\text{on}} - \Delta T_{\text{off}}), \quad (2)$$

where \dot{m} is the mass flow rate, h_{avg} is the bulk enthalpy, V is the arc voltage, I is the arc current, T and c_p are the coolant temperature and specific heat, and the subscripts of ΔT refer to a measurement of the temperature rise with the arc on and with the arc off. This is required to account for the coolant temperature rise that results from pumping a viscous fluid through the cooling lines. An uncertainty analysis for typical measurement errors can be performed, and this indicates that the average total gas enthalpy can be determined fairly accurately.¹⁵ However, there are some important considerations. First, the larger the facility, the more difficult it is to accurately measure the coolant temperature rise. Either a large number of measurements must be made in the smaller coolant lines or the temperature distribution in a large manifold must be resolved to determine the coolant temperature rise. Second, the energy balance does not account for further heat losses beyond the nozzle that may reduce the bulk enthalpy value of the free stream. Finally, although knowledge of the enthalpy determined from an energy balance is important and useful from a facility perspective, it is still an average, or bulk value. This average enthalpy value may not be representative of that part of the test stream actually impinging on the test article since gradients in flow enthalpy that may develop in the arc column persist owing to short residence times in the high pressure region of the nozzle. Perhaps more importantly, the energy balance approach provides no information about the degree of nonequilibrium or how the energy is apportioned in the free stream.

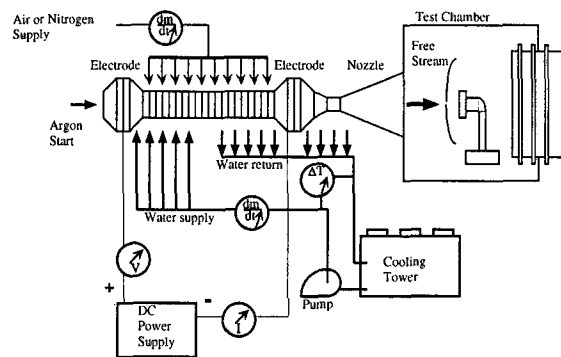


Fig. 7. Energy balance on a large-scale, constricted-arc arcjet test facility.

Energy balance measurements can also be used to determine heater efficiency values during facility operation. The heater efficiency, which is generally a function of arc pressure and current, is defined as

$$\eta_H(p, I) = \dot{m} h_{\text{avg}} / (VI). \quad (3)$$

Once this is determined for the particular heater configuration, it can be used to quickly estimate the bulk enthalpy using the mass flow rate of the gas and the arc voltage and current by simply rearranging the equation. Because the efficiency is a function of the arc current and the stagnation pressure, this measurement must be carried out over the full range of facility operation to develop an empirical correlation that accounts for the dependence.¹⁶ It is important to understand that changes in electrode configuration, or indeed, variation in electrodes themselves will directly influence the heater efficiency. Moreover, the electrodes are typically the most frequently replaced component of the facility, so efficiency values, and this approach to estimating bulk enthalpy, should be used with caution.

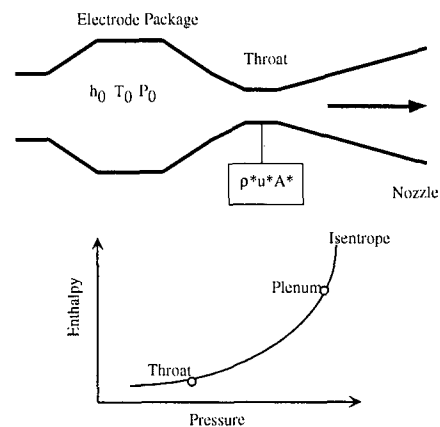


Fig. 8. Sonic flow method for determining enthalpy in an arcjet facility (after Winovich¹⁷).

Sonic Flow - Another method used to determine the total enthalpy is the sonic-flow method that was developed by Winovich.¹⁷ The basic physical principle of this method is that for any given equilibrium thermodynamic state there is a unique value of the sonic mass flow. Thus for a given enthalpy and pressure there is

only one value of the choked mass flow. Conversely, for a known pressure a measurement of the mass flow determines the enthalpy. The graphical representation of this approach is shown in Fig. 8. Assuming that the flow is one-dimensional and in equilibrium, then for both real and ideal gases a simple expression relating mass flow and reservoir enthalpy can be derived from the equations governing the flow from a reservoir through a choked nozzle,

$$\frac{\dot{m}}{(A p_0)} = \frac{\sqrt{2 h_0}}{(R T_0)} \left[\frac{\rho^*}{\rho_0} \left(1 - \frac{h^*}{h_0} \right)^{1/2} \right] \quad (4)$$

In the above expression, A is the cross-sectional area, the subscript 0 refers to stagnation conditions, and the superscript * refers to conditions at the throat.

Simplified versions of this equation can be derived for the case of thermally and calorically perfect gases, as well as for calorically imperfect gases. For real gases both γ and R vary with temperature and pressure and there are no simple closed form expressions that represent this variation. Consequently, the governing equations for the choked nozzle flow were solved iteratively using an equation of state representing a dissociating gas for a range of pressures and enthalpies. For the range of pressures investigated (0.25 to 100 atm) all solutions for the mass flow fell within 4 % of a mean curve. A curve fit procedure was then used to develop the empirical correlation,

$$\frac{\dot{m}}{(A p_T)} = \frac{C}{h_T^{3.97}} \quad (5)$$

where C is a constant factor whose value depends on the system of units. The effects of boundary layer, nonequilibrium (or frozen) chemistry, and variable heat loss to the nozzle walls were examined in the original work pertaining to this measurement approach.¹⁷ While boundary layer and heat loss effects appear to be small, the existence of nonequilibrium flow at the throat leads to a systematically low estimate of the flow enthalpy. As with the energy balance approach, the total enthalpy determined with the sonic-flow method represents an average value, and there is no information about the degree of nonequilibrium where testing takes place beyond the nozzle exit.

Stagnation Point Heat Flux - With certain assumptions the total stream enthalpy can be inferred from a simultaneous measurement of heat transfer and impact pressure at the stagnation point of a blunt body, such as a sphere or cylinder as depicted in Fig. 9. Boundary layer equations for stagnation point heat transfer were developed by Fay and Riddell,¹⁸ and a subsequent modification of these results to include nonequilibrium boundary layer chemistry and surface catalytic effects was given by Goulard.¹⁹ Later, Pope²⁰

presented an experimental investigation of Goulard's theoretical results for arcjet flows. During the same time period, empirical correlations for stagnation point heat transfer in any gas were published:^{21,22}

$$\Delta h = \frac{q}{\kappa} \sqrt{\frac{R_{eff}}{p_p}}, \quad (6)$$

where κ is a gas species dependent constant, R_{eff} is the effective radius of the blunt-body article, and Δh is the difference between the stream and cold wall enthalpy. A clear advantage of this approach is that it gives a spatially resolved measure of the stream enthalpy at the test location. However, an important assumption in the use of the above correlation is that the catalycity of the surface of the heat flux gauge is essentially full, i.e. all atoms impinging on the surface recombine and deposit the excess energy from the exothermic reaction on the surface as heat. It should be noted that full catalycity is rarely achieved for calorimeters, and heat flux measurements with gauges of different catalycity show wide variation.^{23,24} Oxidized, uncleaned surfaces, which are typical on calorimeters that are in service, have significantly lower catalycity. This means that calorimeters will generally under-measure the incident heat flux when significant dissociated species are present at the calorimeter surface. Since the inferred enthalpy is linearly dependent on the measured heat flux, this approach will lead to a lower estimate of the stream enthalpy level.

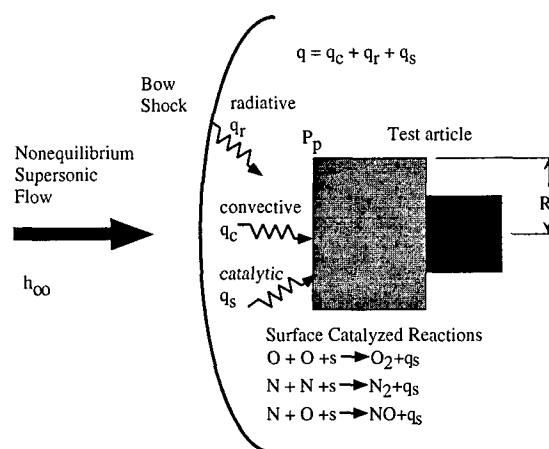


Fig. 9. Stagnation point heat transfer measurements.

All of the conventional approaches to arcjet stream characterization that have been discussed in this section share common attributes in that they infer enthalpy from other flow property measurements and they provide no information on the degree of nonequilibrium. The ability of measurements made using these approaches to guide and inform flow modeling is therefore limited. Furthermore, it is not possible to use these measurements to relate the arcjet stream conditions to the intended flight application, because

they do not address the nonequilibrium state of the free stream.

New spectroscopic techniques that are currently under development may improve this situation, and some of these approaches will be discussed in the second lecture. Judicious application of CFD codes may also improve this situation by providing more insight into the thermochemical state of the flow. However, any CFD codes that are developed for this purpose must be guided by experimental results, and this topic is addressed in the following sections.

2. CFD for Arcjet Flows

Today, CFD is an important resource for aerospace vehicle design, testing, and development. Investigations into new, or poorly understood, flow problems are often undertaken with a combined experimental and computational approach. Both the experiment and the modeling benefit from the collaboration, since the CFD simulations can evaluate a wide parameter space quickly and efficiently, while the experimental results provide guidance for developing assumptions and improving model fidelity. The general state of CFD for a particular discipline in the wider field of aerospace applications is periodically reviewed. Recent reviews that are relevant to simulating arcjet facility flows can be found in Refs. 25 and 26, which examine CFD for high enthalpy test facilities and external flows, respectively.

The present discussion is concerned mainly with the impact of experimental measurements and instrumentation on modeling, so detailed examinations of numerical methods, particular models, and grid resolution, which are familiar topics in the literature regarding CFD, will not be covered. Rather, the intent is to discuss shortcomings in current instrumentation and available experimental data that make the task of producing credible arcjet flow simulations exceedingly difficult, if not impossible. Although the conservation equations and general numerical method are discussed briefly below, they are invoked only to frame the discussion about what must be measured and how well. The perspective is that of an experimental approach to flow modeling that examines assumptions, model inputs, and constraints in order to propose better experimental tests to resolve ambiguities and uncertainties.

2.1 Motivation for Arcjet Flow Modeling

A major driving force behind arcjet flow modeling is the desire to extract the most information from tests of thermal protection systems in large-scale arcjet facilities. Testing costs are always a concern, and an investment in computational resources to avoid test article failures or to conduct a more efficient test cycle

represents a prudent strategy. Computational investigations can often be undertaken at lower expense than experimental efforts. Unless a complete computational capability is being started from scratch, the costs of employing state-of-the-art instrumentation for experimental investigations is usually much higher, assuming that manpower for both efforts is equivalent. If more and better information could be obtained from arcjet testing, then substantial development cost savings may be realized from a reduced dependence on flight experiments (e.g. FIRE^{27,28} and Apollo²⁹) that are often required to establish thermal protection system effectiveness.

Minimizing thermal protection mass for current, low-budget planetary missions is also an important motivation for generally improving the state of knowledge of arcjet flow stream conditions. For these missions there is neither time nor budget for flight testing a prototype before launching. If results from arcjet tests can be extrapolated to flight conditions with quantifiable uncertainties, then it may be possible to reduce the design safety margins that currently added to heat-shield thickness.³⁰ It may ultimately be possible to establish flight performance of thermal protection materials through arcjet testing if a sufficient understanding of arcjet flows is developed. CFD modeling would play an indispensable and enabling role in this effort.

Facility improvements and optimization for particular test configurations could also benefit from the development of CFD tools tailored to arcjet flow modeling. As noted above, ARCFLO played an important role in the early development of large-scale arcjet test facilities, and there is a need for modern computational tools to improve electrode designs, optimize heater configurations, and design new nozzles for flat-plate test configurations. These tools could also be used to design test configurations that would provide the necessary information at reduced cost and effort.

Additional motivation derives from the desire to improve the general state of nonequilibrium flow modeling and the understanding of real gas effects. As mentioned above, the stable, relatively long-duration arcjet operation at high enthalpies creates opportunities for studying complex chemical and thermal interactions that cannot be easily analyzed in impulse facilities.

2.2 CFD Requirements for Arcjet Flow Simulations

Before discussing measurement requirements for improving computational simulations of arcjet facility flows, it is useful to examine the CFD requirements that have evolved from previous and ongoing efforts to model arc-heated flows in large-scale facilities. Arcjet flows are typically not in thermal and chemical equilibrium, except possibly in the constrictor and electrode

package regions. Consequently, any attempt to model the flow requires a CFD code that models nonequilibrium processes.

The conservation equations for hypersonic flows in thermal and chemical nonequilibrium that are solved by the LAURA CFD code³¹ have been compiled in a single reference publication by Gnoffo and his coworkers.³² Eleven species that are typically encountered in simulations of hypersonic air flows were included in the model: N_2 , O_2 , NO , N , O , N_2^+ , O_2^+ , NO^+ , N^+ , O^+ , and e^- . Thus, eleven species continuity equations and three momentum equations must be solved by the code. For this particular CFD code, three separate energy equations are modeled to account for nonequilibrium effects: vibrational energy, electronic energy, and total energy. Thermodynamic data for the eleven species and reaction rates for two different models, Park³³ and Dunn and Kang³⁴, were also given in the report. In this CFD approach, which is representative of those currently in use for nonequilibrium, hypersonic flows, only the ground electronic states of each species are modeled. When radiative energy flux is important, it is typically treated separately or in a loosely-coupled fashion. It should be emphasized that there is no universally agreed upon model formulation, particularly when it comes to nonequilibrium processes and chemical reaction and energy transfer rates. Interested readers are referred to Refs. 35-38 for other computational model formulations.

For arcjet flows in large scale facilities, argon must also be considered since it is often added to the test gas flow to protect electrode surfaces. If only the neutral state is considered, this brings the total number of species for air/argon flows to twelve. In addition, thermodynamic and chemical reaction rate data must also be included for argon.³⁹

2.3 Strategies for Arcjet Flow Simulations

Just as there is no universally accepted model for nonequilibrium, hypersonic flows, there is no single CFD code that can simulate the complete arcjet facility flow from the heater to the test article. Thus, some reasonable modeling strategy must be developed that matches available CFD models to flow regions in an advantageous manner. To illustrate this point, several modeling efforts that were concerned with either arcjet characterization or interpretation of arcjet test results are surveyed below. The presentation is organized by flow region, starting from the heater and moving through the nozzle to the test article.

Arc Heater - The flows within the arc heater and electrode packages are special cases, since the electrodynamic processes occurring within these typically subsonic flow regions are usually absent in hypersonic flows (with the exception of MHD device flows). However, a discussion of numerical studies of arc heaters

is included here for two reasons: first, the flow may be in thermal and chemical equilibrium within the downstream electrode package; and second, if the flow and discharge physics can be modeled correctly, then it may be possible to compute inlet conditions for use in nozzle calculations.

Within an arc-heater, the flow is typically subsonic and is more properly described as a plasma owing to the presence of the electrical discharge. To model this portion of the flow accurately, a coupled solution of the fluid dynamics, radiation, and electrodynamics is required. The development of a CFD model for the arc heater that included the necessary coupling was undertaken at Ames Research Center several years ago,^{40,41} but the effort was eventually abandoned. Instead, the flow within constricted-arc heaters is still modeled with either the ARCFLO code, which was mentioned above, or a derivative. One of the derivative codes, SWIRLARC,^{42,43} has been modified to include the tangential component of gas injection that is typically used to help stabilize the discharge in high-pressure facilities. It should be noted that in any form, ARCFLO does not attempt to fully simulate the physical processes within the heater. Rather, ARCFLO and its derivatives employ a semi-empirical approach to perform comparative studies and indicate trends that might be useful for design studies.

Recently, there has been renewed interest in improving computational models of constrictors. A Navier-Stokes formulation for a constrictor was developed and implemented by Kim et al.,⁴⁴ and an improved, fully-coupled radiation model was applied to the study of an arc heater by Sakai et al.⁴⁵ The main motivation for this renewed activity is the need to increase the efficiency and performance capabilities of existing arcjet facilities. Obviously, measurements will be required to validate these newer flow models.

Nozzle and Free Stream - For studies relating to arcjet characterization, arcjet test interpretation, or general nonequilibrium flow modeling, the expanding flow in an arcjet facility nozzle presents a challenge to the computational community. The general strategy for modeling arcjet nozzle flows relies on some means for estimating the inlet conditions for the nozzle, particularly the stagnation enthalpy, and then using whatever experimental information is available from the free stream to assess the fidelity of the simulation. Depending on the particular computational model, the inlet conditions can be specified either in the subsonic flow region upstream of the throat or in the supersonic portion of the nozzle. As was mentioned in the description of a typical arcjet facility, the nozzle flows are not in thermal or chemical equilibrium. Therefore, the computational approach must model the thermodynamic and chemical kinetic processes that govern hypersonic, nonequilibrium flows.

There have been several efforts aimed at simulating flows in arcjet nozzles. At Ames Research Center alone, three different numerical approaches have been used recently to simulate nozzle flows in conical⁴⁶⁻⁴⁸ and semi-elliptic⁴⁹ geometries. These particular studies were undertaken specifically to address arcjet characterization issues. Additional investigations of conical nozzle flows have been carried out in support of arcjet surface catalysis experiments.⁵⁰ Details of the different numerical approaches are given in each of the references. However, it is interesting to note the progression of the numerical models used in these studies. Babikian used a quasi-one-dimensional, multi-temperature flow model, NOZNT,⁵¹ to compare with free stream temperature measurements in the Ames AHF Arcjet Facility.⁴⁶ Gökçen performed simulations of the nozzle flow with an axisymmetric, nonequilibrium Navier-Stokes solver in support of shock layer experiments.⁴⁷ More recently, Loomis and his coworkers used GASP, which is a general three-dimensional, flow solver to simulate both conical and semi-elliptic nozzle flows in support of thermal protection material tests for the X-33.⁴⁹

Concurrent experimental and computational studies of expanding, N₂/Ar plasma flows have also been carried out by Schönemann and coworkers.⁵² The noteworthy aspect of this particular investigation was the use of experimental measurements at one axial location to start the calculations and predict the rapidly expanding flow properties at a second, downstream location. This approach has the advantage of avoiding some of the uncertainties that result from estimating inflow conditions.

Flow Over a Test Article - As the current use of large-scale arcjet facilities is aimed primarily at simulating aerothermal heating, it is extremely important to be able to model the flow over a test article accurately. Test article flows can be classified into two basic types: shock-layer flows over a test article in a conical nozzle flow and boundary-layer flow over a flat plate for semi-elliptic, or rectangular, nozzle flow. Since the flat plate is usually an extension of the nozzle wall, the modeling requirements for simulating boundary layer flows are identical to those for nozzle flows, although the angle of attack is typically varied as part of an experimental investigation. Shock-layer flows are different, particularly for studies of stagnation point heating. For this configuration, the flow undergoes compression by a shock wave, whose strength depends on the particular test conditions and geometry, before impinging on the test-article surface. Thus, the free stream conditions, which largely determine the characteristics of the shock layer flow, must somehow be known to carry out the simulation.

Typically, there are no stream measurements, other than pitot pressure and heat flux, that could be used

to specify the stream conditions. For certain arcjet test conditions, it is possible to estimate the stream conditions using a combined equilibrium and frozen-flow analytical approach, and then carry the analysis through the shock layer based on measurements of the pitot pressure, heat flux, and model surface temperature.⁵⁰ However, a more general approach involves simulating the nozzle flow (again, an estimate of the initial enthalpy is required) with a numerical model and then using those conditions as input to a shock layer calculation. An example of this latter approach can be found in the work of Gökçen,^{47,48} which will be discussed in detail below. Inevitably, inaccuracies in modeling the expanding nozzle flow affect the simulations of shock-layer and boundary-layer flows in arcjet facilities.

The response of the test article to the shock layer flow is also of considerable interest to the arcjet test and material development communities, where much can be gained by understanding the interaction between the shock layer flow and the material. A review article by Milos and Rasky⁵³ outlines the importance of properly defining the boundary conditions that govern the interactions at the fluid/surface interface. The authors also point out that since boundary processes define the interaction of the fluid and solid computational models, their boundary conditions must agree. This issue is especially important for understanding the performance of charring and ablating thermal protection materials. Although it is very interesting, this topic is outside the scope of the present discussion.

Measurement Requirements for Arcjet Flow Modeling		
Arcjet Flow Measurements		Model Development Measurements
Starting Conditions	Simulation Validation	Three-body recombination rates Third-body efficiencies Spontaneous emission rates Laser-excitation rates Collisional-radiative model rates Species thermodynamic data Energy Transport Rates
Enthalpy Pressure Mass flows of test gases Inflow velocity Contaminant level Turbulent or laminar? Gradients Assessment of equilibrium	Velocity Species concentrations Density Pressure Translational T Rotational T Vibrational T Electronic state populations Post-nozzle expansion rate Stream profiles	

Fig. 10. Classification of measurements for arcjet flow modeling.

3. Measurement Requirements for Arcjet Flow Modeling

Measurements that can be used to improve computational models of arcjet flows can be separated into general categories, which are illustrated in Fig. 10. The first classification distinguishes between direct measurements of properties of arcjet flows and more generic measurements that can influence the development of models for nonequilibrium, hypersonic flows. Measurements of thermodynamic properties, species concentrations, velocity, and enthalpy in arcjet flows

would all fall into the first category of direct measurements. More accurate determinations of important reaction or energy transfer rates, which need not be measured in arcjet flows, would fall into the second category. While this category is probably of equal importance in the improvement of arcjet flow modeling, the majority of the discussion below is concerned with direct measurements of primary arcjet flow quantities.

Within the first category of direct arcjet flow property measurements, a further distinction can be made between measurements that would be used to define starting, or inflow-boundary, conditions and measurements that could be used to assess the fidelity of the simulation. Since the success of any flow modeling effort is inextricably linked to the accuracy with which the starting conditions for the calculation are defined, measurements of the input parameters are considered to be of greater importance. Of the inflow parameters for arcjet flows, the total enthalpy is the most important because it defines the total flow energy and the initial composition and temperature. Despite its importance, enthalpy has proven to be the most difficult parameter to characterize accurately, as discussed above. Typically, the settling chamber pressure is measured to reasonable precision for most arcjet tests, so it is assumed herein that pressure is given. Other primary measurements that define the starting conditions are the mass flows of the test gases and the configuration and geometry of the facility.

Velocity, species concentrations, temperature(s), static pressure, and density are examples of flow property measurements that can be made at various locations in the arcjet to assess the performance of a computational model. Flow quantities that are derived from measurements of primary flow variables, such as the dynamic pressure, specific heat ratio, Mach number, and Reynolds number, are less important from the perspective of evaluating computational models. However, these quantities are quite useful in specifying the performance of the arcjet facility and for relating the test conditions to the expected flight environment.

3.1 Enthalpy

It is readily apparent from even a casual reading of the previous section on modeling requirements that all simulations of the most important arcjet regions, the nozzle and shock-layer, or boundary-layer, flows, require knowledge of the stagnation enthalpy. The state of enthalpy determination using conventional instrumentation was examined in the introductory section, and it was found to be inadequate for several reasons. First, the conventional means for determining the flow enthalpy can only give an estimate of the total value, which does not specify the state of the essentially frozen free-stream flow. Second, for the energy balance and sonic flow approaches, only the bulk enthalpy

value can be determined. While this is useful for monitoring facility performance, the enthalpy value probably does not represent the free-stream core flow, where stagnation-point tests are conducted, unless there are no spanwise enthalpy gradients. The assumption of gradient-free flow appears to be questionable.²⁵ Third, even when great care is taken with the treatment of the calorimeter surface, enthalpy values derived from heat flux measurements are likely to be systematically low.

It should be noted that the measurements required for determining flow enthalpy vary with flow region. Moreover, the influence of the enthalpy determination on the outcome of the flow simulations also depends on where the enthalpy measurement is made. For arc heater and nozzle flow simulations, a measurement of the stream enthalpy within the downstream electrode package, which also functions as a nominal settling chamber, is appropriate. However, for shock layer simulations, inaccuracies are accumulated from simulating both the nozzle flow and the shock layer flow. A more appropriate enthalpy measurement location would be the free stream, provided that the measurement could quantify both the total enthalpy and the nonequilibrium state of the gas. With this information about the free stream, the shock layer flow could be simulated independently of the nozzle flow. Obviously, owing to the nonequilibrium nature of the flow, more flow property measurements are required to determine the thermodynamic and chemical state of the flow in the free stream.

Finally, any enthalpy measurement must be spatially resolved, and enthalpy gradients must be quantified to remove potential ambiguity from the specification of the starting conditions. This issue will be discussed further below and the applicability of nonintrusive optical diagnostics to enthalpy measurements will be addressed fully in the following lecture.

3.2 Arc Heater

The flow within the arc heater and electrode package is usually subsonic and the enthalpy is mostly static, being comprised of thermal and chemical mode contributions. Because pressure is reliably known, a measure of total density or temperature would permit a determination of the total enthalpy. Of the two variables, temperature is more amenable to measurement through optical means. Assuming that the flow is in thermal equilibrium, then determination of a single temperature is sufficient for determining enthalpy. If there is optical access to either the heater or electrode package region, then a spectrally resolved emission measurement can be used to determine temperature. The specific procedures for determining temperatures from spectrally resolved emission are discussed in the following lecture.

Useful information could also be derived from additional measurements of other flow variables in the electrode package. These other flow properties include: the axial flow velocity; the azimuthal velocity component, which would quantify the amount of swirl at the nozzle inlet; the total heat flux and radiative heat flux to the wall; the amount of copper, which is introduced into the stream by the process of electrode erosion;⁵⁴ and the electron number density downstream of the arc. Although the axial extent of the electrode package region is usually not that large, the flow is cooling as it moves toward the throat. Consequently, a determination of the axial variation in any flow quantity would provide some insight into the evolution of the flow as it begins to accelerate.

Owing to limited accessibility, flow probes are not a viable option. Their survival at typical large-scale arcjet facility operating conditions is also an issue. Optical access to the downstream electrode package can often be realized,⁵⁵ and measurements in this region are particularly useful because this region provides the inflow to the nozzle. It may be possible to implement optical measurements at two different axial locations downstream of the arc termination to assess the rate of evolution of the stream properties. Furthermore, since large fluctuations in the magnitude of emission from atomic transitions have been observed in the electrode package,⁵⁵ it may be possible to develop a two point correlation approach for velocity measurement.

3.3 Arcjet Nozzle and Free-Stream Flow

Nozzle - For the purposes of this discussion, the starting point for nozzle flow is defined as the end of the electrode package. Unlike the segmented arc heaters and electrode packages of today's constricted-arc facilities, the nozzle assemblies are typically fabricated in a more monolithic manner. Because they are fabricated with integral water cooling, there is little hope for instrumenting existing large-scale arcjet nozzles. This essentially precludes *in situ* monitoring of the onset of chemical and thermal freezing, which could then be used as a starting point for frozen flow analysis.

Using smaller scale arcjet devices fabricated with segmented nozzles it may be possible to address the onset of chemical, and possibly thermal, freezing for flow conditions of interest in aerothermal testing applications. Note that the fluid dynamic expansion rate plays an important role in determining the location at which the flow freezes. Whatever studies are undertaken in smaller facilities must address this issue.

Free Stream - Although the flow is usually chemically and thermally frozen by the time it exits the nozzle, the free stream region is often optically accessible, and measurements of many flow properties are possible. Spatially resolved measurements of velocity, translational temperature, density, pressure,

and species concentrations have all been made using laser-induced fluorescence (LIF) techniques.⁵⁶⁻⁵⁹ Recently, measurements of enthalpy and its distribution among thermal, chemical, and kinetic modes, were demonstrated in N_2/Ar ⁵⁸ and air/ Ar ⁵⁹ flows using two-photon LIF of atomic nitrogen. Although more property measurements are required to determine enthalpy for nonequilibrium flow, the approach of using LIF of the dissociated species to determine multiple flow parameters appears capable of providing this information with the aid of certain assumptions. Fortunately, the validity of the assumptions that are currently invoked can be evaluated experimentally.⁵⁹ Flow property measurements using LIF techniques will be discussed extensively in the second lecture.

Although further development of this approach is required to assess the assumptions and establish the range of applicability, LIF based stream property measurements may ultimately prove sufficient to establish the enthalpy and degree of nonequilibrium of the free stream flow. This would provide a set of inflow conditions that could be used to calculate the shock-layer flow. A computational simulation of the flow over a test article that was started from known free stream conditions and compared to shock-layer property measurements would allow a better assessment of the computational modeling. Determinations of free stream rotational and vibrational temperatures and assessments of possible metastable atomic state populations are needed to establish the validity of the LIF-based approach.⁵⁹

In addition to establishing inflow conditions for shock layer simulations, the two-photon LIF measurements provide stream property information that can be used to evaluate the fidelity of nozzle flow simulations. Since total enthalpy is specified by the LIF measurements, with a quantified uncertainty, that value can be used along with the constrictor pressure to start the nozzle simulation. If the model used in the nozzle flow simulation is accurate, it should reproduce the measured distribution of the total enthalpy into kinetic, thermal, and chemical contributions in the nonequilibrium free stream. Comparisons between nozzle simulations and free stream measurements are underway for the chemically simpler N_2 /argon flow cases.

3.4 Blunt-Body Shock-Layer Flow

Even with the free stream conditions specified, much is required in order to improve the general understanding of shock-layer flows in the stagnation-point heating configuration for aerothermal test applications. Finite rate effects that vary in significance depending on the test conditions and model geometry still control the chemical and thermal state of the shock layer and impact issues such as the difference in catalytic heating between the arcjet test conditions and the flight environment. Moreover, depending on the test geometry

and conditions, merged shock layer and rarified flow effects may be important, and may complicate the interpretation of heat transfer data.

Instrumentation and techniques for making spatially resolved flow property measurements are therefore required to establish the thermochemical state of the gas in the shock layer as it moves toward the surface of a test article. Spatial resolution is important because the flow is generally evolving from a nonequilibrium state toward an equilibrium state as it approaches the surface. Understanding this evolution is important from a modeling perspective as well as for aiding in the interpretation of test results. Again, for nonequilibrium situations, multiple flow properties, including velocity, species concentrations and temperatures must be measured to specify the flow state. In contrast to free stream conditions, shock layer temperatures (T_r , T_v , and T_e) can reach levels in excess of 5000 K and pressures can be orders of magnitude higher. Many internal energy levels of a number of species will be populated, and the distributions of populations over these energy levels may differ for different species (and possibly electronic states). With an ablating material, the situation is even more complex.

However, the goal of understanding the shock layer thermochemistry is important because that is the environment that must ultimately be related to flight conditions. In addition, if instrumental approaches that determine the thermochemical state of the shock-layer can be developed, then it may be feasible to test all-body vehicle configurations in the long-duration, arcjet flow facilities.

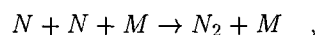
3.5 Measurement Accuracy Requirements

The uncertainty in experimental measurements and in computational predictions is an important consideration in arcjet flow investigations. For the present discussion, only uncertainties in experimental measurements are considered. Experimental uncertainties are estimates of errors in measurements that typically arise from either systematic or random contributions, or more typically, both. The systematic and random contributions are manifestations of the more general measurement attributes: accuracy and precision. Definitions of measurement accuracy and precision, which are frequently confused, can be found in a variety of reference publications, including a text on the subject by Bevington.⁶⁰ In the introductory discussion, Bevington indicates that the accuracy relates to how close a measured value is to the "true" value, while precision provides information on how well something can be measured, regardless of what that measurement means. For arcjet flow property measurements that would be used to improve flow modeling capabilities, both accuracy and precision are important. However, because flow properties are generally unknown, instrumentation must be developed to make measurements

with a minimal reliance on assumptions that cannot be tested; otherwise it is impossible to assess accuracy. How closely a measured flow property represents the real situation is important from the perspective of predicting absolute flow property magnitudes, as in the simulation of a single arcjet test.

In contrast, it is often easier to establish the precision of a particular measurement from a number of different observations at similar conditions. This can be done without evaluating all of the assumptions that may go into a particular measurement, and it may then be possible to use the measured quantity constructively without knowing the absolute accuracy. Once the precision is established, then the measurement could be made for a number of different flow conditions where a single control parameter, such as the arc current, is varied. Simulations of these different flow conditions and comparisons with the experimental results would test the ability of the model to predict trends and might ultimately do more to establish confidence in the modeling than single-condition comparisons. Obviously, the model would have to be optimized for an appropriately chosen test condition. This approach may prove to be more effective in advancing both modeling and instrumentation development, especially when one considers the number of measurements required to document a single test case completely. As the instrumental techniques mature and as more is learned from parametric comparisons, then it may be feasible to pursue a single, well-documented test case.

From an experimental perspective, given the scarcity of data and the fact that measurement results from one facility cannot be directly transferred to another unless the configuration is identical, any property measurements that also have quantified uncertainty estimates are useful in advancing the general state of knowledge. Enthalpy measurements, as well as other inflow conditions that are required to initiate simulations, are examples of this type of flow property. Measurements that are used to evaluate the validity of computational models must be held to a higher standard, since their determination may influence changes in the model formulation. It is difficult to formulate a general statement as to how high the standard should be, given the complexity of present day CFD models. For some parameters an accuracy requirement can be postulated easily. As an example, consider LIF-measured atomic nitrogen concentrations, which currently have an estimated uncertainty of $\approx 30\%$.⁵⁹ Although this uncertainty appears to be large, the recombination rate for the reaction,



which largely determines the N atom concentration in the chemically frozen free stream, is currently uncertain by up to a factor of three.⁶² Clearly even the

relatively uncertain N atom concentration measurement can be used to evaluate flow model performance. To determine accuracy requirements for other flow properties, an effort should be made to evaluate uncertainties in quantities currently used in the models and parametric studies with the computational model should be performed to evaluate sensitivities.

4. Experimental and Computational Investigation of Shock-Layer Flows

Recent attempts to simulate arcjet flows and compare the numerical predictions with experimental measurements illustrate the current status of both simulations and measurements. Knowledge gaps that affect the comparisons between simulations and measurements are readily apparent. The combined experimental and computational investigation of blunt-body, shock-layer flows in the Ames AHF Arcjet Facility was chosen for this purpose because the investigation was motivated by the need for improved characterization of arcjet flows, and understanding the shock-layer flow is directly relevant to aerothermal testing of thermal protection materials. Although experimental investigations have also been undertaken in the electrode package and free stream regions of the same arcjet facility, comparisons between measurements and simulations for those studies are ongoing. Consequently, more can be learned from examining the process and the results of the documented shock-layer flow property comparisons, and from the results of those comparisons.

4.1 Objectives of Investigation The objectives of this investigation were to: 1) determine whether a region of thermal and chemical equilibrium exists in the shock layer formed over a flat-faced cylinder; 2) determine the conditions required to establish the equilibrium region; and 3) determine whether or not enthalpy measurements could be derived from spectrally resolved emission emanating from the equilibrium region.

Early investigations of arcjet facility flows included efforts to characterize the shock layer flow using emission spectroscopy.^{62,63} If the flow is in thermal and chemical equilibrium, then a measurement of the temperature from spectrally resolved emission and a concurrent pressure measurement would uniquely specify the thermochemical state of the flow and its enthalpy. A relatively recent analysis of shock-layer emission appeared to indicate the presence of an equilibrated region within the shock layer at a lower pressure than had been expected.⁴⁶ Therefore, a major goal of the present investigation was to verify the existence of the equilibrated region, and begin the task of defining the conditions that produce the equilibrium flow. By undertaking this investigation, issues associated with the development of an "enthalpy meter" based on mea-

surements of shock layer emission could also be assessed.

At the outset, several areas of uncertainty were identified that had to be addressed in the investigation. These areas included: 1) what criteria are used to identify a region of thermal and chemical equilibrium; 2) how to interpret emission measurements with certainty; and 3) the effects of spatial intensity gradients on measurements that are integrated along the line-of-sight. It quickly became apparent that computational-flow modeling could address some of these issues and help guide the experimental investigation. Conversely, it was realized that the experimental measurements might also provide some assessment of the computational model validity, but this was not the primary objective.

4.2 Experimental and Computational Approach

Experiment - The shock layer emission experiments were carried out in the Ames AHF Arcjet Facility, which was previously described in the introductory section. To generate the highest shock layer pressure values the facility was configured with the 30.5 cm diameter nozzle, which produces the least free stream expansion. A 15.2 cm diameter, flat-faced cylinder made of copper was placed in the stream to generate the shock layer. Two different test conditions were surveyed, and these are referred to as the high pressure and low pressure cases. Test conditions for the two cases are summarized in Table 1.

Table 1. Arcjet test conditions for shock layer investigation.

Test Conditions			
Case	Pressure	Current	Voltage
	atm	A	V
Low	1.70	1141	2657
High	6.80	2075	5630

To obtain as much information from a single facility run as possible, line-of-sight emission spectra were acquired from multiple axial locations along the central stagnation streamline using a spectrograph and CCD camera. The model was placed at two different axial locations in the stream, 34.5 and 36.9 cm downstream of the nozzle exit (forward and back positions, respectively), to allow full coverage of the shock layer emission with the finite viewing area of the CCD and spectrograph system. Thus, two separate facility runs at the same nominal operating conditions were required to obtain the full shock layer emission profile for each test case.

Emission spectra were acquired at several grating positions covering the UV to near-IR wavelength range and the measured signals were converted to absolute intensities through calibration with standard spectral lamps. Each grating position was chosen to measure

certain spectral features that could be used to ascertain temperature or species information using spectral analysis techniques.^{64,65} Particular attention was given to developing methods for determining rotational and vibrational temperatures using spectral feature ratios that minimized the influence of uncertainties in the measurements. This was desirable because agreement between the measured temperature values was thought to be a good indicator of the presence of a thermally equilibrated flow region. Portions of the N_2^+ (1,2), (0,1), and (0,0) vibrational bands were found to yield vibrational and rotational temperatures with minimum uncertainty based on spectral simulations. Note that the temperature values are derived from emission that is integrated along the line-of-sight, so the inferred flow properties actually represent intensity-weighted, spatially averaged values. Further details of the experimental configuration and the spectral analysis can be found in Refs. 65 and 66.

Computational Modeling Approach - The experimental measurements consisted of spectrally resolved, absolute intensities from multiple axial locations within the shock layer during a single facility run. Consequently, the computational simulation had to be able to address issues relating to emission, which required the use of a radiative transport code. In addition, two different CFD models were required to predict the shock layer flow. The first model was used to simulate the nozzle flow to determine the free stream conditions ahead of the shock layer, which was then simulated with a second, separate computational model. Flow properties predicted by the shock layer model were then used to calculate the radiative transport.

The two flow models that were used for the simulation were developed by Gökçen.^{67,68} Both models use an axisymmetric formulation, which is appropriate for the conical nozzle flow and the shock layer flow over a flat-faced cylinder. Twelve chemical species: N_2 , O_2 , NO , N , O , N_2^+ , O_2^+ , NO^+ , N^+ , O^+ , e^- , and Ar ; are modeled for these flows, and three temperatures: translational, rotational, and vibrational; are used to represent the thermal state of the gas mixture. The reactions and rate coefficients that are used in the model are derived from the multi-temperature model of Park and Lee.⁵¹ Turbulence is not included in either flow model; the flow is assumed to be laminar throughout the facility. Further details of the computational models can be found in Refs. 67 and 68, and more information about the nozzle and shock layer computations can be found in Refs. 47 and 48.

To calculate the emissive flux for the shock layer flow, the NEQAIR⁶⁹ radiative transport model was used. Inputs to the model, which include species concentrations and temperatures, were obtained from the flow solution by interpolating between calculated quantities

at the known measurement locations. For all of the calculations, the emitting level populations were assumed to follow Boltzmann distributions, albeit with potentially differing values of rotational and vibrational temperatures. The electronic temperature was assumed to equal the vibrational temperature.

Starting Conditions for the Calculations The most important inputs to the CFD model are the starting conditions, and, as discussed above in the introductory section, the flow enthalpy and its spatial distribution are not known in the free stream or at the entrance to the nozzle. Therefore, some means of estimating the starting conditions based on facility measurements was required for the nozzle and shock layer simulations. For this investigation, measurements of stagnation point heat flux and shock layer pitot pressure were used to estimate the total stream enthalpy based on an empirical correlation of the form presented in Eq. (6). At the time of this work, the argon mass flow rate had not been recently measured, so it was assumed to be equal to 5 % of the total mass flow for the high pressure case. Using the estimates of flow enthalpy and argon mass flow along with the facility measurement of the arc heater pressure, the nozzle flow could be calculated. Based on the low level (≈ 3 ppm) measured in the stream of the 60 MW arcjet facility,⁹ copper was not included in the simulations of the AHF arcjet nozzle and shock layer.

Upon exiting the nozzle, the flow regions that are within the local Mach angle near the periphery expand into the test box at a rate that is different from that in the nozzle, unless the nozzle exit static pressure matches the ambient pressure. Owing to this further expansion, the calculated flow property values at the exit of the nozzle could not be used directly as the inflow conditions for the shock layer simulations. This effect is well documented for perfect gas flows,⁷⁰ but the rates of expansion for the nonequilibrium arcjet flows at various operating conditions are not known. Therefore, the calculations were continued in the axial direction at the nozzle expansion rate until the calculated dynamic pressure matched the value derived from the shock layer pitot pressure measurement using Eq. (1). Although this procedure does not exactly reproduce the fluid dynamics of the full free stream, it produced acceptable inflow conditions for the shock layer simulations without requiring a complete simulation of the flow in the test box.

It should be noted that the enthalpy value that was ultimately used in the simulations was greater than the value derived from the stagnation point heat flux and pressure measurements for both the high and low pressure test cases. After performing initial comparisons between the calculated and measured emission spectra, the enthalpy was increased for both test cases to bring the calculated spectra into closer agreement

with the measurements. The total increase for the high pressure case was limited arbitrarily to 10 %, although it could have been increased further, as will be seen below. Adjusting the total flow enthalpy estimate to a higher value is justified if the calorimeter surface has a low catalycity and the recombining atom flux is significant, because correlations such as Eq. (6) apply to fully catalytic surfaces. While the catalycity of the particular calorimeter used for these measurements is not precisely known, the surface of the constantan foil was known to have a ceramic oxide coating, so the gauge was considerably less than fully catalytic. Given the uncertainty in the total flow enthalpy, the poor agreement found in the initial comparisons between calculated and measured spectra could not be attributed to the flow model. This clearly illustrates the importance of quantifying the stream enthalpy, since using the experimental measurements to guide the adjustment of the input conditions compromises any assessment of the flow model.

4.3 High Pressure Case

Calculated Shock-Layer Properties - Using the inflow conditions and two-model computational approach the flow properties were calculated for the shock layer at the high pressure case conditions. Axial profiles of the flow properties along the central streamline where the measurements were made are shown in Fig. 11 and 12. The axial distributions of pressure and temperature are shown in Fig. 11 as a function of non-dimensionalized distance from the test article surface. Note that the nozzle solution predicts that the flow is vibrationally frozen ahead of the shock, but the rotational energy is predicted to be in equilibrium with translation. The rotational and translational temperatures rise significantly near the shock and decrease as the blunt-body surface is approached. A lesser increase is exhibited by the vibrational temperature, and all three temperatures are seen to converge to a value that is very close to the equilibrium temperature for these conditions at about 0.1 R upstream of the surface. Thus, the calculations suggest that there is a region of thermal equilibrium within the shock layer at the high pressure conditions.

Axial profiles of species mass fractions are shown in Fig. 12, also as a function of the normalized distance upstream of the test article surface. Outside of the surface boundary layer, at the point where the temperature values converge, the species mass fractions are quite close to their equilibrium values, which are indicated on the right-most vertical axis. According to the simulation, the flow is also very nearly in chemical equilibrium at these test conditions.

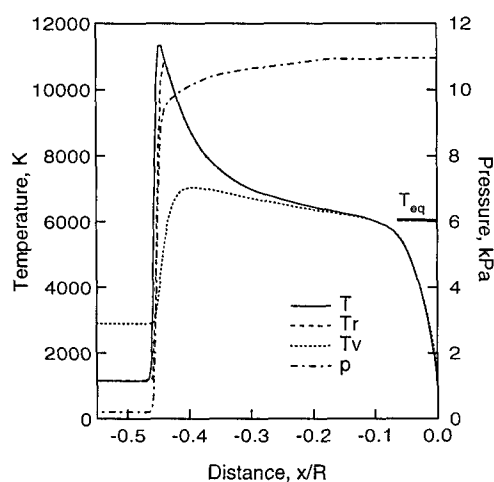


Fig. 11. Temperature and pressure profiles within the shock layer for the high pressure case.

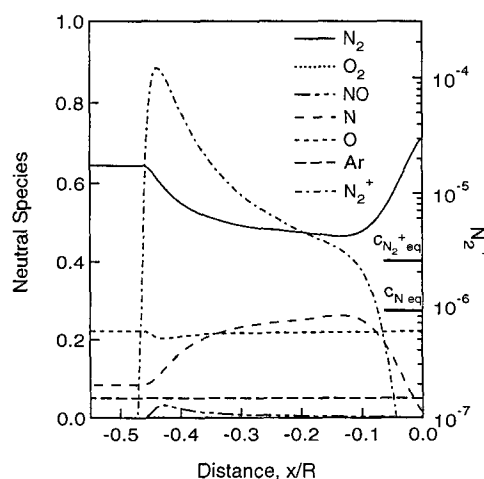


Fig. 12. Species mass fraction profiles within the shock layer for the high pressure case.

In the description of the experimental effort above, the use of N_2^+ spectral features to determine vibrational and rotational temperature values within the shock layer was noted. For an isolated rovibrational transition, the measured intensity for thermal equilibrium conditions can be expressed as

$$I_\lambda = \frac{K_\lambda n L}{Q} e^{-E_u/kT}, \quad (7)$$

where I_λ is the spectral intensity, K_λ represents the line shape function and the transition strength, n is the species density, Q is the partition function, L is the line-of-sight path length, and E_u is the total upper state energy. This expression shows that the intensity has a linear dependence on the emitting species density and an exponential dependence on temperature. From the computed axial property profiles of Figs. 11 and 12, it is apparent that all temperatures and the N_2^+ concentration are higher near the shock front. Consequently, the measured N_2^+ emission could

easily be dominated by contributions from emission at the shock front, where nonequilibrium effects are more likely to be present. Temperatures are derived from intensities with the implicit assumption that the rotational and/or vibrational level populations are each thermally equilibrated. If the measured intensity is dominated by emission from nonequilibrium regions, then this assumption is untenable.

The prediction of significantly higher temperatures and N_2^+ concentrations near the shock front led to a further analysis of the flow property distributions along the emission measurement sight lines. Recall that one of the objectives was to use temperature measurement comparisons to determine whether or not the flow reached thermochemical equilibrium. This requires that the temperature values derived from the spectral analysis actually represent the central, core-flow region, rather than the shock front. To assess this potential problem in interpreting the spectral data, computed flow property profiles along the spanwise flow direction were extracted from the shock layer solution at selected axial measurement locations.

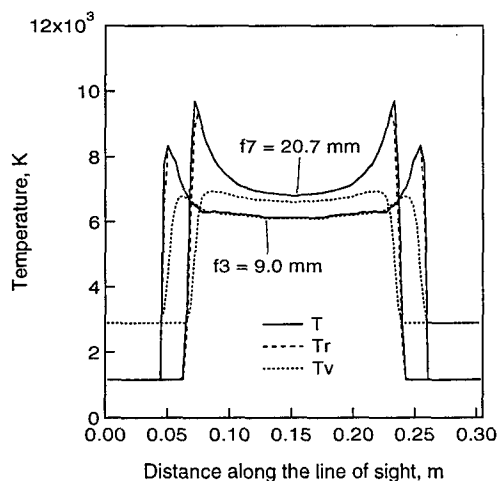


Fig. 13. Temperature variation along the line-of-sight for the high pressure case.

Profiles of rotational and vibrational temperatures along the line-of-sight direction, which is normal to the flow axis, are shown in Fig. 13 for two of the measurement positions. The axial location of the sightlines is given on the figure in terms of the distance from the surface of the test article. Again, this will make it difficult to draw conclusions about the state of the flow from temperatures derived from the emission spectra.

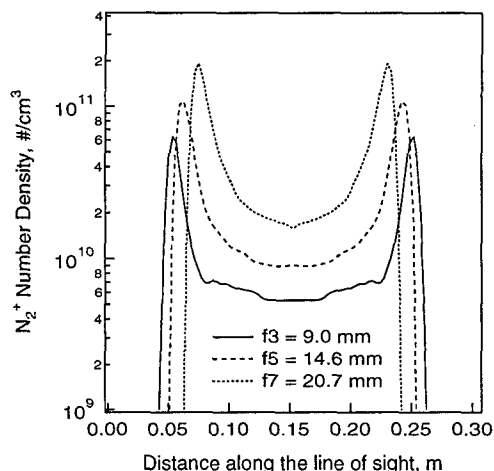


Fig. 14. N_2^+ number density along the line-of-sight for the high pressure case.

Computed N_2^+ number densities are shown in Fig. 14 as a function of distance along the line-of-sight at three different axial measurement locations, two of which correspond to the locations of the temperature profiles in the previous figure. As with temperatures, there is a significant increase in N_2^+ number density near the shock front. For the two flow properties that govern emission from N_2^+ , the shapes of the spanwise profiles are predicted to be far from the idealized top hat distribution that is assumed to exist in the spectral analysis.

Comparisons With Measurements - Despite the indication that strong spatial gradients would compromise the derivation of flow properties from the measured intensities, values of line-of-sight integrated rotational temperature, vibrational temperature, and number density values were extracted from the spectral data. To make a meaningful comparison, the calculated flow field emission was averaged in the same manner as the measured intensity. The approach used to derive these values from the flow property and emission calculations is described at length in Ref. 47.

Comparisons of the measured and calculated line-of-sight (LOS) averaged temperatures are shown in Fig. 15. Measured and calculated vibrational and rotational temperatures are shown as a function of the normalized distance from the surface of the test article. Despite the predicted strength of the shock-front region emission, the computed, LOS-averaged temperatures still appear to nearly converge near the test article surface. Compared to the measured temperature values, the computed LOS averaged values appear to approach convergence faster and to a greater degree. Although the overall trends appear to be consistent between the measured and calculated values, the two sets of LOS-averaged temperatures do not agree. In view of this disparity and because the measured temperature values do not converge, the existence of an

equilibrated flow region could not be ascertained from the comparison.

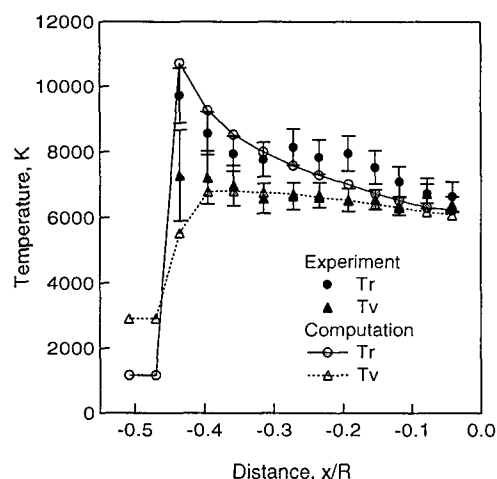


Fig. 15. Predicted and measured line-of-sight averaged temperatures for the high pressure case.

By assuming that the vibrational temperature determined from the spectral analysis of the measured intensities represented the electronic temperature, values of LOS-integrated N_2^+ number density could be determined. As was done for temperature, an approach for deriving a comparable quantity from the calculated flow properties was also developed.⁷¹ Measured and calculated values of the LOS-integrated N_2^+ number density are compared in Fig. 16. Some of the disagreement between the two sets of number densities can be attributed to differences in spatial gradients along the line-of-sight. Until the spatial gradient effects are investigated experimentally, it is not possible to determine whether the difference seen in the comparison nearer the test-article surface is caused by spatial averaging from the optical system or by inaccurate modeling of the N_2^+ dissociative recombination processes.

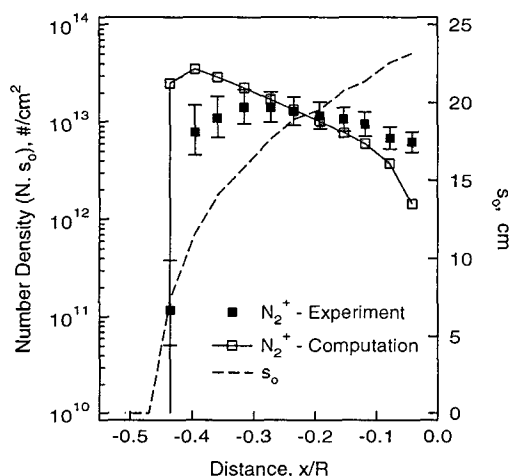


Fig. 16. Predicted and measured LOS-integrated N_2^+ number density for the high pressure case.

Based on the comparisons between the measured and calculated flow properties above, it was not possible to determine whether an equilibrated flow region exists within the shock layer for these conditions. Such a determination clearly requires an approach that resolves the spatial intensity gradients to extract information from the relevant flow region in the core of the shock layer. Once that is done, then the impact of other assumptions can be examined, and the processes that lead to equilibration can be investigated. Although the question of an equilibrated region was not conclusively resolved, it was still possible to address whether or not emission-based measurements could be used to determine the thermochemical state of the flow.

For these investigations, the experimental instrumentation did not actually measure flow properties. Instead, flow property information was derived from an analysis of measured emissive intensities. To address the issue of using emission to evaluate the flow enthalpy and to understand how the experimental approach and the computational modeling might be improved, comparisons were made between calculated and measured spectral data at selected measurement locations.

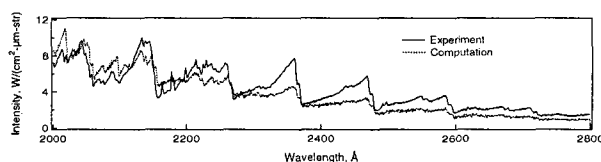


Fig. 17. Measured and computed emission spectra for the 240 nm grating position, 20.7 mm upstream of test article.

Comparisons between the measured and calculated emission spectra are presented below at several grating positions for a single axial location, 20.7 mm upstream of the test article. For the 240 nm grating position, the comparison is shown in Fig. 17. At this spectral location, the emission is mainly from NO γ and δ with probable contributions from the β and ϵ systems. Owing to the overlap of the emission from the different electronic states of NO, extracting temperature information from this spectral region is not feasible. Except for emission below 2100 Å, the calculated intensity is less than the measured value.

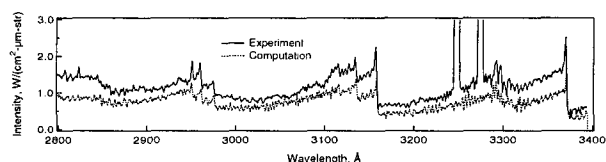


Fig. 18. Measured and computed emission spectra for the 310 nm grating position, 20.7 mm upstream of test article.

A similar comparison of measured and calculated emission spectra at the 310 nm grating position is shown in Fig. 18. The off-scale spectral features are Cu atom

transitions. Copper is present in the stream because of electrode erosion, and it is not included in the computational model. Emission from molecular species in this spectral region is mainly from NO at shorter wavelengths, and $N_2(2+)$ and $N_2^+(1-)$ systems at the longer wavelengths. The strongest emission peaks aside from those due to Cu emission are from $N_2(2+)$. Agreement between the calculations and the measurements is reasonable good in shape, but the overall signal level from the computational spectra appears to be low. Recall that the calculated signal levels are exponentially dependent on the electronic temperature. If the calculated electronic temperature, which is nearly 6000 K at this measurement location, was increased by 200 K, the $N_2(2+)$ emission would nearly double.

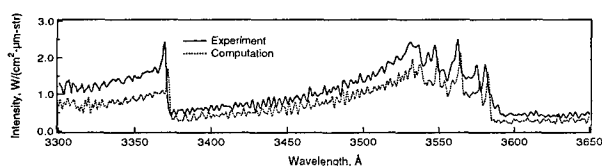


Fig. 19. Measured and computed emission spectra for the 345 nm grating position, 20.7 mm upstream of test article.

For the 345 nm grating position comparison, which is shown in Fig. 19, the emission is mainly from molecular species: $N_2(2+)$, $N_2^+(1-)$, and CN violet. The CN in the flow comes from dissociation of CO_2 that is present naturally in air and the subsequent recombination of C and N. Although it is truly a minor species, the transition strength is large and it is a significant emitter, as seen in the region near 3550 Å where several of the measured peaks are not reproduced by the calculated spectra. Cyanogen was not included as a species in the computational model. Some of the under-prediction of the intensity magnitude can therefore be attributed to the exclusion of CN from the calculation. For the $N_2^+(1-)$ emission, a 200 K increase in the electronic temperature would produce a roughly 20 % increase in the calculated intensity.

Comparisons were also done for the 415 and 450 nm grating positions, which contained mostly molecular emission, and the agreement between the measured and calculated intensity magnitude is better, although the calculated levels are still low. The improved agreement for these grating positions is likely due to their use to guide the adjustment of the estimated stream enthalpy.

The shock layer flow also contained significant O and N atom populations, and atomic transition intensities were recorded at two near-IR grating positions. The measured and computed emission from O atomic transitions at 777 nm and 845 nm are compared in Figs. 20a and 20b. As with the grating positions at the shorter wavelengths, the calculated intensity is generally lower than the measured intensity. At a calculated

electronic temperature of 6000 K, an increase of 200 K would nearly double the atomic emission.

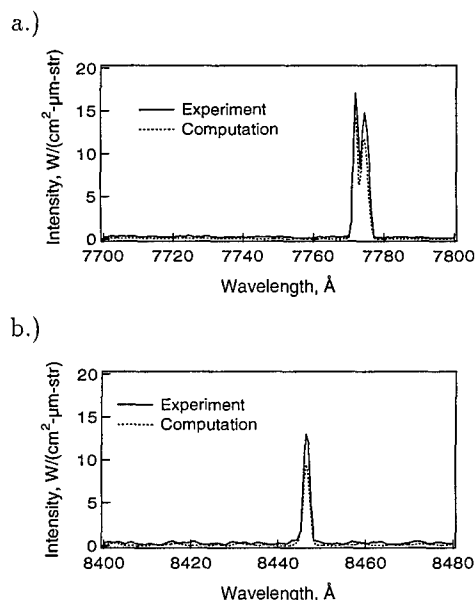


Fig. 20. Measured and computed emission from the a) 777 nm O transitions and from the b) 845 nm O transition, 20.7 mm upstream of test article.

Similar comparisons were done for N atom transitions and these are shown in Fig. 21a and 21b for the 744 and 868 nm N transitions, respectively. The calculated emission for the N atom transitions is also low and because the emitting states are at energy levels that are similar to those of the O atom transitions above, an increase in the electronic temperature of 200 K would also result in a near doubling of the intensity for these transitions.

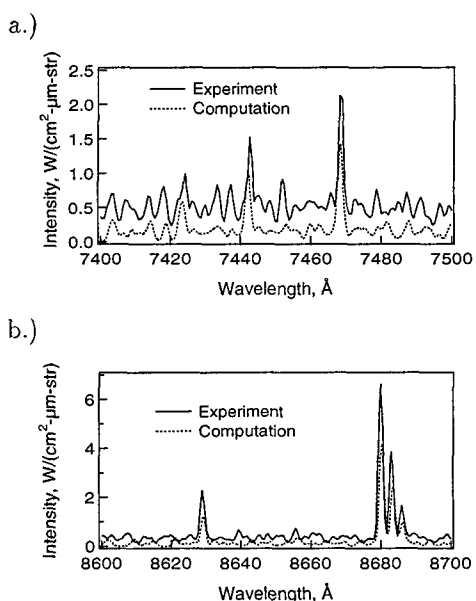
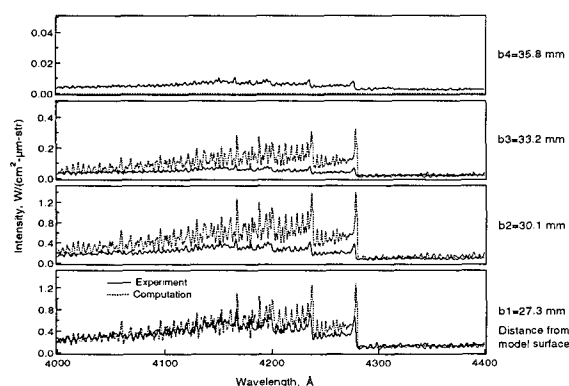


Fig. 21. Measured and computed emission from the a) 745 nm N transition and from the b) 868 nm N transition, 20.7 mm upstream of test article.

Based on these spectral comparisons, it appears that the calculated emission was generally low for all grating positions at this measurement location. Since the emission is exponentially dependent on temperature, it is likely that the calculated flow temperature was low. Again, the most likely culprit for this discrepancy is the enthalpy, which was probably not raised to the proper level. Clearly, the exponential dependence of the emission on temperature makes emission a very sensitive indicator of flow temperature. From an instrumentation development perspective, this implies that emission-based measurements have both the signal magnitude and sensitivity that are necessary to measure temperature, and ultimately flow enthalpy (with the assumption that velocity is negligible within the shock layer), reasonably well. However, the spatial gradients must be resolved for this approach to succeed.

A different perspective on the LOS-integrated N_2^+ number density distribution that was presented in Fig. 16 can be obtained by comparing measured and calculated N_2^+ (1-) emission for a single grating position at each of the measurement locations on the central stagnation streamline. This comparison is shown for the 426 nm grating position in Fig. 22a for the back position of the test article, and in Fig. 22b for the forward position. There is an easily distinguishable difference between the evolution of the measured signal and the calculated signal. By performing a direct comparison of measured and calculated emission spectra, uncertainties introduced in the analysis that was performed to derive flow properties from measured intensities are avoided. However, possible differences between measured and calculated flow property gradients are still present and will influence the comparison. Of particular concern is the possibility of additional averaging of the measured intensities that may have been caused by the optical collection system.⁶⁵ This possibility has not been accounted for in these comparisons, so only qualitative statements can be made regarding the differences between the calculated and measured spectra.

a.)



b.)

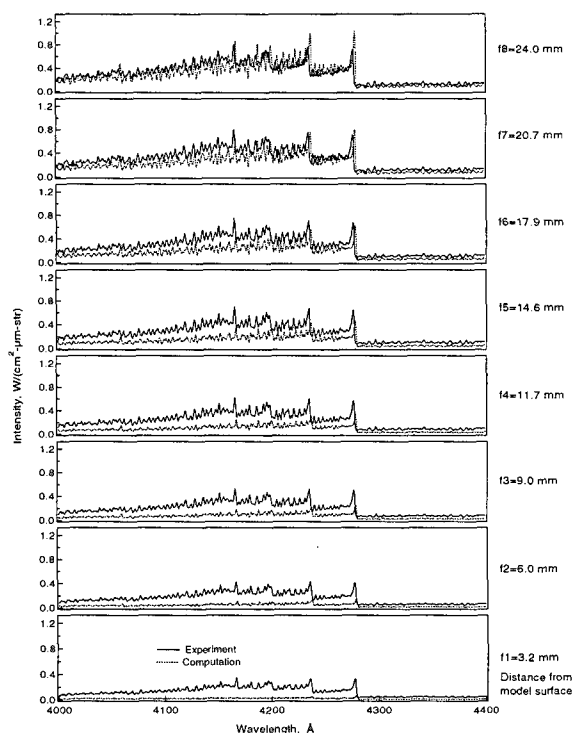


Fig. 22. N_2^+ emission at 420 nm grating position for all of the axial measurement locations for the high pressure case: a.) back position; b.) forward position.

In Figs. 22a and 22b, it is apparent that the measured rate of evolution and decline of the N_2^+ emission as the flow goes from the shock to the test article is less rapid than predicted by the calculations. Although the limitations in the spatial resolution of the optical system preclude further statements about the axial distribution of the N_2^+ emission, the comparison does illustrate the possibility of using emission spectra to evaluate the population dynamics of important shock layer species.

4.4 Low Pressure Case

Starting Conditions - The lower pressure case test conditions were chosen to maximize the change in shock layer pressure, which was reduced by a factor of ≈ 3 . At the lower pressure, the collision frequency in the shock layer is reduced significantly. Consequently, the flow is less likely to be in thermal or chemical equilibrium. If the degree of departure from equilibrium could be determined at these test conditions, then progress could be made in defining the test conditions that lead to equilibration within the shock layer.

As was found in the comparisons between the simulated and measured emission spectra for the high pressure case, the comparisons for the low pressure case indicated that the stream enthalpy value derived from the stagnation point heat flux and pressure measurements was probably low. Therefore, additional calculations were performed at total enthalpy values that were 14 % and 32 % higher than the estimated values.

In addition to the uncertainty in the stream enthalpy that was present for both the high and low pressure test cases, the uncertain argon mass flow rate became an issue for the simulations of the low pressure conditions. The total mass flow rate for the low pressure case was reduced by a factor of ≈ 4 , based on the reduction in pressure, while the start and shield argon mass flow remained constant. For the high pressure case, the argon mass flow was assumed to be 5 % of the total mass flow. This implied that the relative argon mass flow could be 20 % of the total mass flow for the low pressure case. At this level, the uncertainty in the argon mass flow becomes more important because of its increased participation in the reaction kinetics. For example, in three-body recombination reactions, Ar is less efficient than N_2 as the third body.⁶¹ To address this additional uncertainty and attempt to bound its influence, flow simulations were performed for three different argon mass fractions: 5 %, 10 %, and 30 %.

Thus, owing to the uncertain starting conditions a total of five different simulations of the shock layer flow for the low pressure case were computed. The starting conditions and computed free stream properties for each of these simulations are summarized in Table 2. At nearly constant enthalpy, increased argon mass flow is seen to increase the temperatures and free stream velocity slightly, while increasing the dissociation fraction for nitrogen substantially. Comparing cases that have the same argon mass fraction, increasing the total enthalpy produces results that are similar to increasing argon mass fraction at constant enthalpy. This uncertainty in the starting conditions clearly create difficulties for comparisons of simulations and experimental measurements.

Table 2. Starting conditions and free stream properties for the low pressure test case simulations

Parameter	Case 1	Case 2	Case 3	Case 4	Case 5
p_0 , atm	1.7	1.7	1.7	1.7	1.7
h_0 , MJ/kg	15.2	15.15	17.15	17.26	20.07
w_{Ar}	.05	.30	.05	.30	.10
u_∞ , km/s	4.12	4.19	4.29	4.39	4.53
p_∞ , Pa	62.	57.5	58.5	57.1	57.6
T_∞ , K	727	775	741	823	786
$T_{v\infty}$, K	2960	3360	3100	3550	3370
w_{N_2}	.67	.45	.63	.42	.53
w_N	.06	.09	.10	.12	.16
w_O	.22	.16	.22	.16	.21

Calculated Shock-Layer Properties - Using the Case 3 conditions, axial profiles of temperatures and pressure for the shock layer flow were computed, and these are shown in Fig. 23 as a function of the normalized distance from the test article surface. While the rotational and translational temperatures are still higher near the shock, the increase over the levels nearer the test article is not as great as was seen for

the high pressure case (see Fig. 11). At the lower shock layer pressure, the vibrational and translational-rotational temperatures do not appear to converge outside of the boundary layer of the test article. This is in contrast to the results of the simulation for the high pressure case, where the temperatures clearly converged as the model surface was approached. According to the simulation, the shock layer is not in thermal equilibrium, except within the boundary layer at these simulated conditions.

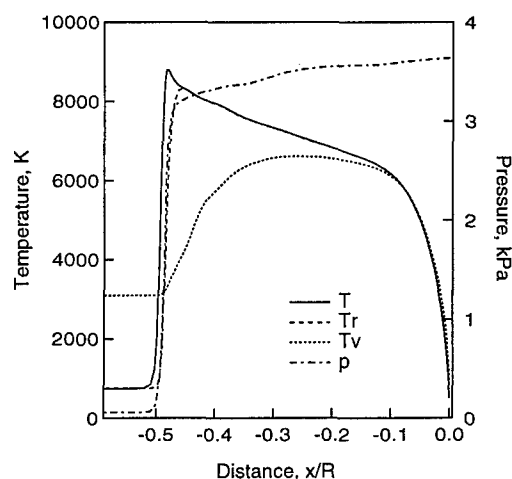


Fig. 23. Axial profiles of temperature and pressure in the shock layer.

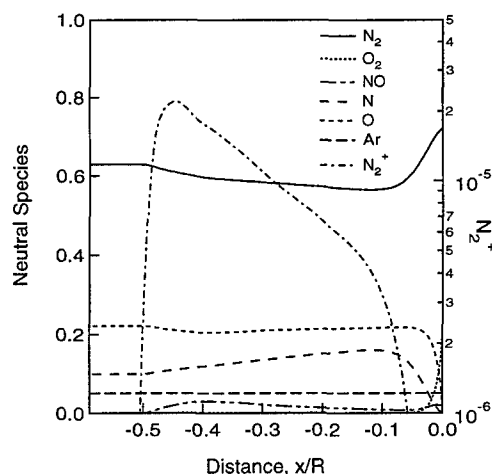
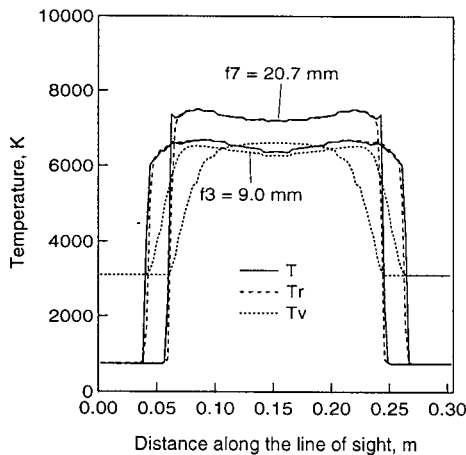


Fig. 24. Axial profiles of species populations in shock layer.

For the same starting conditions, the axial profiles of the neutral species and N_2^+ are plotted in Fig. 24, again as a function of the nondimensional distance from the surface. As was seen in the high pressure case, there appears to be a significant peak in the N_2^+ concentration near the shock front. However, for the low pressure conditions of this simulation, the mass fraction near the shock front is only ≈ 5 times higher than the mass fraction nearer the test article surface (as opposed to ≈ 50 times for the high pressure case, see

Fig. 12). The mass fractions of N and N_2 do not reach a limiting value as the surface is approached, so the simulation indicates that the shock layer is also not in chemical equilibrium.

a.)



b.)

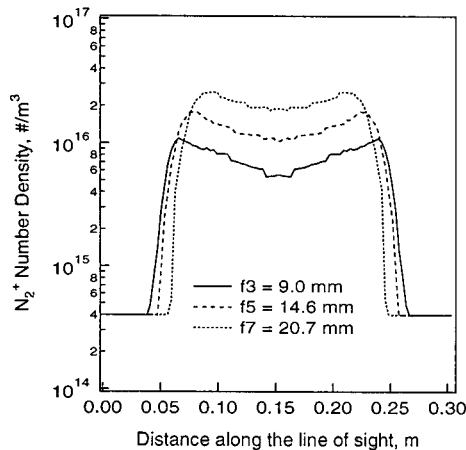


Fig. 25. Computed flow property profiles for Case 3 conditions at selected axial locations for a) temperatures and b) N_2^+ number density.

Although the starting enthalpy and argon mass flow values were less certain for the low pressure case, the gradients in the N_2^+ and temperature profiles appeared to be less severe than found for the high pressure case. To assess the spatial gradients along the optical sight lines at the measurement locations, temperature and species profiles were extracted from the shock layer solutions, and these are shown for selected axial locations in Figs. 25a and 25b, respectively. For both temperatures and N_2^+ number density, the computed profiles along the lines-of-sight are much closer to the idealized top-hat distributions that are required to derive temperatures that are representative of the core flow region from the spectral analysis of the measured intensities. Unfortunately, it appears that the majority of the shock layer flow is likely to be in nonequilibrium, which may violate the other major assumption

of the spectral analysis. The degree of departure from equilibrium and its impact on the distributions of populations over the various energy levels is difficult to quantify.

Comparisons With Measurements - As with the high pressure case, rotational and vibrational temperature values were derived from an analysis of N_2^+ spectral features.⁶⁶ Using an intensity-weighted averaging approach,⁴⁷ temperature values that could be compared with the experimental values were extracted from the computed flow properties at the axial measurement locations for some of the different simulation cases. Comparisons between the computed and measured LOS-averaged temperatures are shown in Figs. 26 and 27, for the simulation conditions of Case 3 and Case 4, respectively. For these two cases, the enthalpy levels were in the middle of the range of simulations and were nearly in agreement. However, for Case 3 the argon mass fraction was 0.05, while for Case 4, the argon mass fraction was 0.3. In Fig. 26, for the Case 3 condition, there are significant differences in both trends and magnitudes between the computed and measured temperatures. First, for the experimental values, the rotational and vibrational temperatures do not appear to overlap, except perhaps accidentally at one or two measurement locations. Owing to low signal levels near the shock front, the measured values are highly uncertain. Consequently, the discussion of trends will be restricted to the positions nearer to the surface than $x/R = -0.4$. For those locations, the trends in the computed and measured vibrational temperatures appear to be reasonably similar, although the measured values are generally greater in magnitude. In contrast, the measured rotational temperatures do not appear to decrease significantly from the values near the shock front, while the computed rotational temperatures clearly show evidence of relaxation going toward the test article.

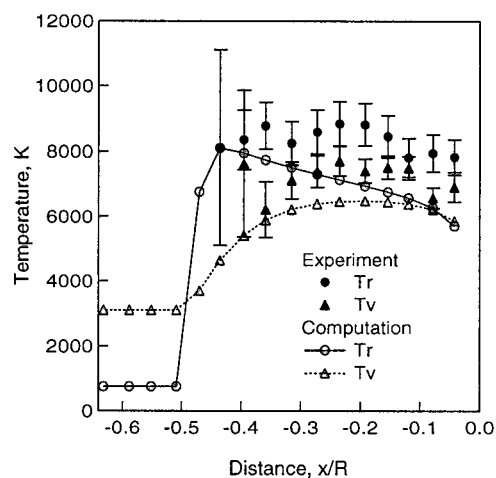


Fig. 26. Computed and measured LOS-averaged temperatures for the conditions of Case 3 ($h_0 = 17.15$ MJ/kg, $w_{Ar} = 0.05$).

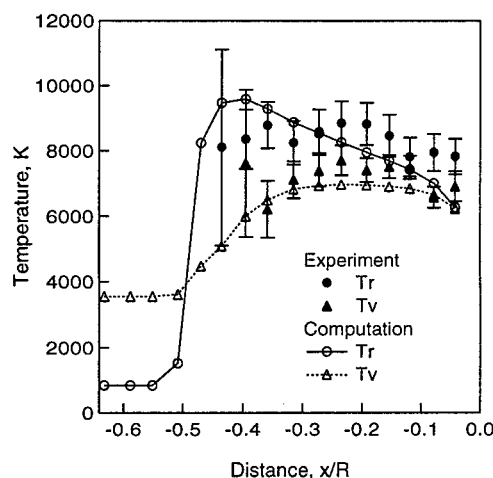


Fig. 27. Computed and measured LOS-averaged temperatures for the conditions of Case 3 ($h_0 = 17.26$ MJ/kg, $w_{Ar} = 0.30$).

At the high argon mass flow conditions of Case 4, the comparison between measured and computed LOS-averaged vibrational temperatures shows improved agreement on the magnitude, while maintaining reasonable agreement on the shape of the distribution at locations closer than $x/R = -0.4$. The agreement between magnitudes of the computed and measured LOS-averaged rotational temperatures also appears to be improved with the increased argon mass flow, but the difference between the distributions is unaffected. It should be noted that the influence of streamwise and spanwise spatial averaging by the optical collection system on the measured values has not been fully accounted for in these comparisons. Considering the uncertainty in the starting conditions for the simulations and the uncertainty in the unresolved spatial intensity gradients for the experiment, the general lack of agreement is not surprising.

4.5 Spatially Resolved Measurements

In a recent set of experiments conducted at the low pressure test conditions, Park acquired emission spectra from multiple locations along the spanwise direction as a single axial position within the shock layer.⁷¹ Several separate emission measurements were recorded simultaneously by the spectrograph and CCD system, and a series of adjusted collection mirror positions were used to cover the radial extent of the shock layer during a single facility run. An Abel-inversion was then used to obtain spatially resolved emission spectra from the LOS-integrated intensities. Finally, temperatures were derived from the Abel-inverted spectra using an analytical method that involved ratios of N_2^+ spectral features and ratios of O atom transitions. A fuller description of the experiment and the analytical approach is given in Ref. 71.

Radial distributions of the rotational, vibrational, and electronic temperatures that were derived from the

spectrally resolved emission are shown in Fig. 28. The rotational and vibrational temperatures were determined using the same analytical approach that was used to derive temperatures from the line-of-sight intensities, above. As explained in Ref. 71, two sets of atomic oxygen transitions were used to calculate electronic temperature. Thus, the two electronic temperature distributions are labeled by the shorter wavelength transition used in each intensity ratio. Owing to an unresolved background contribution at the 8446.5 Å transition, electronic temperatures derived from the intensity of that transition are systematically low. Electronic temperature values obtained using the 7773.4 Å transition are believed to be valid.

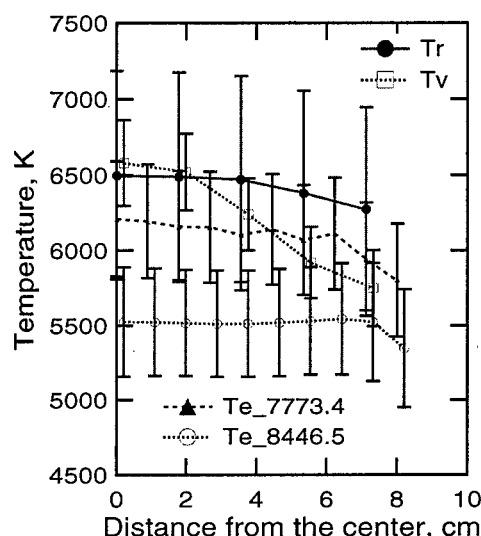


Fig. 28. Radial temperature profiles in the shock layer at 12.7 mm upstream from the test article. Labels for T_e indicate the shorter wavelength O transition of the pair.

The most striking aspect of the radial temperature distribution shown in Fig. 28 is that the rotational, vibrational, and electronic (for the 7773.4 Å pair) temperatures appear to overlap within their respective uncertainties. This may indicate a region of thermal equilibrium within the shock layer for the low pressure conditions, contrary to the prediction of the computational simulation. The shapes of the rotational and vibrational temperature distributions are reasonably similar to the shapes of the predicted radial temperature distributions at 9 mm that were shown in Fig. 25a. (Note that the 9 mm axial location of the predictions was closest to the 12.7 mm axial position of the measurements.) The temperatures and the emission spectra from these experiments are still being analyzed.

4.6 Lessons Learned

First, and foremost, the futility of attempting to perform detailed computational simulations of arcjet flows without adequate specification of the starting conditions, mainly the enthalpy, has to be recognized. Un-

til this issue is resolved, the knowledge gained from performing combined experimental and computational investigations will be marginal. The limitations of using stagnation point heat flux and impact pressure measurements to estimate enthalpy were clearly illustrated. Although the unspecified argon mass flow rate did affect the low pressure test simulations, this inflow parameter is a more tractable problem. Most large-scale arcjet facilities routinely measure the mass flows of the test gases, and the Ames Research Center Arcjet Facilities have recently been equipped with improved mass flow sensors and control capability.

The second important lesson to derive from this exercise concerns the use of diagnostic techniques and approaches that do not resolve spatial gradients. Attempts to compare simulation predictions with measurements of spatially integrated quantities can lead to misleading conclusions. For the low pressure case, the LOS-averaged temperature distributions suggest that the flow is not in thermal equilibrium, while the radial distribution of spatially resolved temperatures suggest the opposite. An investment of additional effort into acquiring emission spectra in the radial direction to obtain Abel-inverted intensities has a far better (and more certain) return than deriving the comparable integrated flow properties from a number of computational simulations. It was fortunate that the comparisons between the predicted and measured LOS-averaged temperatures agreed so poorly for the high and low pressure cases; otherwise, the temptation to "correct" the measurements using the computational results may have proven overwhelming.

Finally, the possibility that a portion of the shock layer is in thermal equilibrium at the low pressure test conditions contradicts the computational predictions, which showed extensive thermal nonequilibrium for all of the different low pressure simulations. Further knowledge of the chemical state of the shock layer, which is currently under investigation, and verification of equilibrium would provide much-needed insight into the nature of the shock layer flow.

5. Summary and Recommendations

The question of the state of CFD simulations of arcjet flows is still dominated by the lack of knowledge about the flow enthalpy. Any other consideration is secondary. Conventional methods for estimating the flow enthalpy, including energy balance, sonic flow, and stagnation point heat transfer, all provide insufficient specification of the flow enthalpy for simulation purposes. If adequate resources and dedicated effort are brought to bear on this problem, then eventually it will be resolved and arcjet facility simulations will become much more meaningful. New LIF-based approaches to enthalpy measurement may improve this situation.^{58,59}

Although this premise cannot be rigorously tested until enthalpy can be more accurately determined, it appears that current nonequilibrium, hypersonic-flow computational models are able to provide reasonable simulations of arcjet flows. This observation is based on a qualitative assessment of the comparisons between the shock layer measurements and predictions, combined with the fact that no obvious shortcomings in the flow models could be identified. Despite having to estimate the enthalpy and use two CFD models and a radiative transport code to predict intensity, the comparisons with measured values were generally favorable; particularly for the high pressure case.

While the flow enthalpy must be accurately specified to enable detailed comparisons between simulations and measurements for a single arcjet facility test condition, measurements and simulations of relative trends in arcjet characteristics are not similarly constrained. Measurements and simulations of the response of sensitive flow properties to changes in arcjet control parameters during a single facility test can add substantial information to the knowledge base at the present time. The approach to this involves using diagnostic instrumentation to monitor stream parameters, when conditions have stabilized, as a single control variable, such as the arc current, is changed. (Examples of this type of experiment will be discussed extensively in the second lecture.) Making the best possible estimate of the total enthalpy for a single condition, a computational simulation is essentially calibrated at that condition. Subsequent conditions are then simulated using further estimates of the total enthalpy, without changing the other parameters of the model. Comparisons are then made between the measured and predicted trends. This approach avoids the larger uncertainties that pertain to measurements of absolute quantities.

Some of the more obvious parametric studies to perform include: 1.) varying pressure to assess impact on chemistry; 2.) varying the arc current, which varies the initial ionization level; and 3.) varying the test gas composition to investigate relative third-body efficiencies in N_2 recombination.

To establish the validity of diagnostic approaches, comparisons between measurements made using multiple independent instruments would be extremely useful. This observation is particularly relevant to developing new approaches for determining the flow enthalpy, which is the most important parameter to measure accurately, and which ultimately determines how useful and relevant arcjet testing will become.

At present, it is too early to propose code validation experiments for large-scale arcjet facility flows. However, it is appropriate to begin thinking about how to develop diagnostics and strategies that may eventually enable code validation experiments in these facilities. The most important advantage that arcjets have over

impulse facilities is the test duration. Steady state flow conditions and material response can be achieved and documented. The long test time allows for multiple property measurements that can be temporally averaged. Because there is no diaphragm, these measurements can be repeated in multiple runs to assess facility repeatability with a rapid turn-around time between tests.

Test guidelines for validation experiments have been suggested by Mehta in his descriptions of methods for producing credible computational simulations.⁷² Performing validation experiments in arcjet facilities will require considerable maturation of currently available diagnostic techniques to ensure adequate specification of inflow conditions for either nozzle or shock-layer flow simulations. In addition to improving the accuracy of inflow condition measurements, sufficient spatial coverage must be attained to allow approximate integration of the flow properties for comparison with other measurements of mass flow, energy balance, etc. Without this type of internal accuracy check of the experimental results, confidence in the measurements would not be sufficient to motivate extensive computational simulations or efforts to improve physical models.

6. Acknowledgements

Many colleagues have contributed to the lecture material contained herein, but special thanks are due to Tahir Gökçen and Chung Park of Thermosciences Institute (Elret), Mark Newfield of Ames Research Center, and James Donohue of UTRC for their excellent work on the combined computational and experimental investigation of arcjet flows. John Balboni of the Thermophysics Facilities Branch at Ames Research Center provided many useful references on arcjet facilities in general. The entire staff of the Aerodynamic Heating Facility Arcjet provided vital test support and Frank Hui's efforts as test engineer deserve special recognition. Many of the thoughts expressed in this document resulted from conversations with colleagues about arcjet flows and testing. While any erroneous statements are attributable solely to the author, the contributions of Chul Park, Joan Pallix, Raj Venkatapathy, Ellis Whiting, and Jochen Marschall of Thermosciences Institute (Elret) to what has been written are greatly appreciated. Similar conversations with Paul Kolodziej, Jeff Bull, Dave Stewart, Joe Hartman, Joe Olejniczak, Dave Olynick, Stephanie Langhoff, Surrendra Sharma, and George Raiche of NASA Ames Research Center have also proven to be very helpful in writing this document.

7. References

1. P. R. Dennis, C. R. Smith, D. W. Gates, and J. B. Bond, Editors, Plasma Jet Technology, NASA

- Report SP-5033, National Aeronautics and Space Administration, Washington, DC, October, 1965.
2. D. A. Gerdeman and N. L. Hecht, Arc Plasma Technology in Materials Science, Springer-Verlag, New York, 1972.
3. H. A. Stine, "The Hyperthermal Supersonic Aerodynamic Tunnel", presented at International Symposium on High Temperature Technology, Asilomar, CA, 8-11 September, 1963.
4. C. E. Shepard, V. R. Watson, and H. A. Stine, "Evaluation of a Constricted-Arc Supersonic Jet", NASA Technical Note TN D-2066, 1964.
5. C. E. Shepard, "Advanced High-Power Arc Heaters for Simulating Entries into the Atmospheres of the Outer Planets", AIAA Paper No. 71-263, AIAA 6th Aerodynamic Testing Conference", (1971).
6. V. R. Watson and E. B. Pegot, "Numerical Calculations for the Characteristics of a Gas Flowing Axially Through a Constricted Arc", NASA TN D-4024, 1967.
7. C. Park, J. H. Lundell, M. J. Green, W. Winovich, and M. A. Covington, "Ablation of Carbonaceous Materials in a Hydrogen-Helium Arcjet Flow", *AIAA J.*, **22**, pp. 1491-1498, October, (1984).
8. J. R. Jedlicka, "The Shape of a Magnetically Rotated Electric Arc Column in an Annular Gap", NASA Technical Note TN D-2155, 1964.
9. W. Winovich and W. C. A. Carlson, "The 60-MW Shuttle Interaction Heating Facility", presented at the 25th International Instrument Symposium, Anaheim, ISBN 87664-434-5, May, (1979).
10. C. Park, "Laboratory Simulation of Aerothermodynamic Phenomena: A Review", AIAA Paper No. 92-4025, AIAA 17th Aerospace Ground Testing Conference, Nashville, TN, (1992).
11. R. K. Smith, D. A. Wagner, and J. W. Cunningham, "A Survey of Current and Future Plasma Arc-Heated Test Facilities for Aerospace and Commercial Applications", AIAA Paper No. 98-0146, 36th Aerospace Sciences Meeting, Reno, NV, 12-15 January, 1998.
12. A. Balter-Peterson, F. Nichols, B. Mifsud, and W. Love, "Arc Jet Testing in NASA Ames Research Center Thermophysics Facilities", AIAA Paper No. 92-5041, *AIAA International Aerospace Planes Conference*, (American Institute of Aeronautics and Astronautics, New York, 1992).
13. C. Scott, "Survey of Measurements of Flow Properties in Arcjets", *Journal of Thermophysics and Heat Transfer*, **7**, pp. 9-24, (1993).
14. H. W. Leipmann and A. Roshko, Elements of Gasdynamics, John Wiley & Sons, New York, 149, (1957).
15. D. A. Gerdeman and N. L. Hecht, Arc Plasma Technology in Materials Science, Springer-Verlag, New York, pp. 94-97, (1972).
16. J. Balboni, Thermophysics Facilities Branch, NASA

- Ames Research Center, private communication, (1997).
17. W. Winovich, "On the Equilibrium Sonic-Flow Method for Evaluating Electric-Arc Air-Heater Performance", NASA TN D-2132, NASA, Washington, DC, 1964.
 18. J. A. Fay and F. R. Riddell, "Theory of Stagnation Point Heat Transfer in Dissociated Air", *J. Aeronautical Sciences*, **25**, pp. 73-85, (1958).
 19. R. Goulard, "Catalytic Recombination Rates in Hypersonic Stagnation Heat Transfer", *Jet Propulsion*, **28**, pp. 733-745, (1958).
 20. R. B. Pope, "Stagnation-Point Convective Heat Transfer in Frozen Boundary Layers", *AIAA Journal*, **6**, pp. 619-626, (1968).
 21. E. V. Zoby, "Empirical Stagnation-Point Heat-Transfer Relation in Several Gas Mixtures at High Enthalpy Levels", NASA TN D-4799, NASA, Washington, DC, (1968).
 22. R. B. Pope, "Measurements of Enthalpy in Low-Density Arc-Heated Flows", *AIAA J.*, **6**, pp. 103-110, (1968).
 23. E. L. Winkler and R. E. Sheldahl, "Influence of Calorimeter Surface Treatment on Heat-Transfer Measurements in Arc-Heated Test Streams", *AIAA J.*, **4**, pp. 717-716, (1966).
 24. L. A. Anderson, "Effect of Surface Catalytic Activity on Stagnation Heat-Transfer Rates", *AIAA Journal*, **11**, pp. 649-656, (1973).
 25. C. Park, "Evaluation of Real-Gas Phenomena in High-Enthalpy Aerothermal Test Facilities: A Review", *J. Thermophysics and Heat Transfer*, **11**, pp. 330-338, (1997).
 26. G. Candler, "Chemistry of External Flows", in *Aerothermochemistry for Hypersonic Technology*, VKI Lecture Series 1995-04, von Karman Institute for Fluid Dynamics, Rhode Saint Genese, (1995).
 27. D. L. Cauchon, "Project Fire Flight I Radiative Heating Experiment", NASA TM X-1222, (1966).
 28. D. L. Cauchon, "Radiative Heating Results from the Fire II Flight Experiment at a Reentry Velocity of 11.4 Km/s", NASA TM X-1402, (1967).
 29. D. B. Lee and W. D. Goodrich, "The Aerothermodynamic Environment of the Apollo Command Module During Suborbital Entry", NASA TN D-6792, (1972).
 30. D. Olynick, Y.-K. Chen, and M. E. Tauber, "Forebody TPS Sizing with Radiation and Ablation for the Stardust Sample Return Capsule", AIAA Paper No. 97-2474, June, (1997).
 31. P. A. Gnoffo, "Application of the Program LAURA to Three-Dimensional AOTV Flowfields", AIAA Paper NO. 86-0565, January, (1986).
 32. P. A. Gnoffo, R. N. Gupta, and J. L. Shinn, "Conservation Equations and Physical Models for Hypersonic Air Flows in Thermal and Chemical Nonequilibrium", NASA TP-2867, February, (1989).
 33. C. Park, "Assessment of a Two-Temperature Kinetic Model for Ionizing Air", AIAA Paper No. 87-1574, June, (1987).
 34. M. G. Dunn and S.-W. Kang, "Theoretical and Experimental Studies of Reentry Plasmas", NASA CR-2232, (1973).
 35. J.-H. Lee, "Basic Governing Equations for the Flight Regimes of Aeroassisted Orbital Transfer Vehicles", in *Thermal Design of Aeroassisted Orbital Transfer Vehicles*, H. F. Nelson, ed., Volume 96 of Progress in Astronautics and Aeronautics, AIAA, New York, pp. 3-53, (1985).
 36. G. V. Candler and R. W. McCormack, "The Computation of Hyperonic Ionized Flows in Chemical and Thermal Nonequilibrium", AIAA Paper No. 88-0511, Jan., (1988).
 37. K. G. Brown, "Chemical and Thermal Nonequilibrium Heat Transfer Analysis for Hypervelocity, Low Reynolds Number Flows", AIAA Paper No. 85-1033, June, (1985).
 38. C. Park, *Nonequilibrium Hypersonic Aerothermodynamics*, John Wiley & Sons, New York, (1990).
 39. R. J. Gessman, C. O. Laux, and C. H. Krueger, "Experimental Study of Kinetic Mechanisms of Recombining Atmospheric Pressure Air Plasmas", AIAA Paper No. 97-2364, AIAA 28th Plasmadynamics and Lasers Conference, Atlanta, GA, June, (1997).
 40. P. Durgapal, "Electrode Phenomena in High Current, High Pressure Arc Heaters", *J. Thermophysics and Heat Transfer*, **7**, pp. 412-417, (1993).
 41. P. Durgapal, "Strongly Coupled Radiative Transfer and Joule Heating in an Arc Heater Cathode", *J. Thermophysics and Heat Transfer*, **8**, pp. 730-736, (1994).
 42. S. F. Shaeffer, "SWIRLARC: A Model for Swirling, Turbulent, Radiative Arc Heater Flowfields", AIAA Paper No. 78-68, (1978).
 43. W. N. MacDermott and E. J. Felderman, "Arc Heater Scaling Parameters Predicted with the SWIRLARC Code", AIAA Paper No. 93-2797, AIAA 28th Thermophysics Conference, July, (1993).
 44. K. H. Kim, O. H. Rho, and C. Park, "Assessment of ARCFLO Code and Computations of Arc Heater Using Navier-Stokes Code", AIAA Paper No. 99-0736, AIAA 37th Aerospace Sciences Meeting, Jan., (1999).
 45. T. Sakai, K. Sawada, and M. Mitsuda, "Application of Planck-Rosseland-Gray Model for High Enthalpy Arc Heaters", AIAA Paper No. 98-2838, (1998).
 46. D. S. Babikian, N. K. J. M. Gopaul, C. Park, "Measurement and Analysis of Nitric Oxide Radiation in and Arcjet Flow", *J. Thermophysics and Heat Transfer*, **8**, pp. 737-743, (1994).
 47. T. Gökçen, C. S. Park, M. E. Newfield, and D. G. Fletcher, "Computational Simulation of Emission Spectra from Shock Layer Flows in an Arc-Jet Facility", *J. Thermophysics and Heat Transfer* **12**, 180-

- 189, (1998); also AIAA Paper No. 97-0135.
48. T. Gökçen, C. S. Park, and M. E. Newfield, "Computational Analysis of Shock Layer Emission Measurements in an Arc-jet Facility", AIAA Paper No. 98-0891, AIAA 36th Aerospace Sciences Meeting, Jan., (1998).
49. M. P. Loomis, S. Polsky, E. Venkatapathy, D. K. Prabhu, and F. C. L. Hui, "Arcjet Semi-Elliptic Nozzle Simulations and Validation in Support of X-33 TPS Testing", AIAA Paper No. 98-0864, AIAA 36th Aerospace Sciences Meeting, Jan., (1998).
50. D. A. Stewart, Y.-K. Chen, D. J. Bamford, and A. B. Romanovsky, "Predicting Material Surface Catalytic Efficiency Using Arc-Jet Tests", AIAA Paper No. 95-2013, AIAA 30th Thermophysics Conference, June, (1995).
51. C. Park and S. H. Lee, "Validation of Multi-temperature Nozzle flow Code", *J. Thermophysics and Heat Transfer*, **9**, pp. 9-16, Jan.-March, (1995).
52. A. T. Schönemann, M. Auweter-Kurtz, H. A. Habiger, P. C. Sleziona, and T. Stöcle, "Analysis of the Argon Additive Influence on a Nitrogen Arc-jet Flow", *J. Thermophysics and Heat Transfer*, **8**, pp. 466-472, (1994).
53. F. S. Milos and D. J. Rasky, "Review of Numerical Procedures for Computational Surface Thermochemistry", *J. Thermophysics and Heat Transfer*, **8**, pp. 24-34, (1994).
54. W. N. MacDermott, D. D. Horn, and C. J. Fisher, "Flow Contamination and Flow Quality in Arc Heaters Used for Hypersonic Testing", AIAA Paper No. 92-4028, (1992).
55. J. M. Donohue, D. G. Fletcher, and C. S. Park, "Emission Spectral Measurements in the Plenum of an Arc-jet Facility", AIAA Paper No. 98-2946, 7th AIAA/ASME Joint Thermophysics and Heat Transfer Conference, June, (1998).
56. D. J. Bamford, A. O'Keefe, D. S. Babikian, D. A. Stewart, and A. W. Strawa, "Characterization of Arc-Jet Flows Using Laser-Induced Fluorescence", *J. Thermophysics and Heat Transfer*, **9**, pp. 26-33, (1995).
57. D. J. Bamford and A. Romanovsky, "Velocity and Chemical Composition Measurements in an Arc Jet Flow", AIAA Paper No. 95-2039, AIAA 30th Thermophysics Conference, June, (1995).
58. D. G. Fletcher, "Arcjet Flow Properties Determined from Laser-Induced Fluorescence of Atomic Nitrogen", AIAA Paper No. 98-0205, 36th Aerospace Sciences Meeting, (1998).
59. D. G. Fletcher and D. J. Bamford, "Arcjet Flow Characterization Using Laser-Induced Fluorescence of Atomic Species", AIAA Paper No. 98-2458, 7th AIAA/ASME Joint Thermophysics and Heat Transfer Conference, (1998).
60. P. R. Bevington, Data Reduction and Error Analysis for the Physical Sciences, McGraw-Hill, New York, pp. 3-7, (1969).
61. D. L. Baulch, D. D. Drysdale, D. G. Horne, and A. C. Lloyd, Evaluated Kinetic Data for High Temperature Reactions, Vol. 2, Butterworth Group, London, pp. 25-53, (1973).
62. W. Winovich, "Total Radiation Measurements at the Stagnation Point of Blunt Bodies at Stagnation Temperatures to 15000 K", AIAA Paper No. 68-405, AIAA 3rd Aerodynamic Testing Conference, April, (1968).
63. A. F. Okuno and C. Park, "Stagnation Point Heat Transfer Rate in Nitrogen Plasma Flows: Theory and Experiment", *Journal of Heat Transfer*, pp. 372-384, August, (1970).
64. C. O. Laux, "Optical Diagnostics and Radiative Emission of Air Plasmas", Stanford High Temperature Gasdynamics Laboratory Report No. HTGL T-288, Stanford University, August, (1993).
65. C. S. Park, M. E. Newfield, D. G. Fletcher, T. Gökçen, and Sharma, S. P., "Spectroscopic Emission Measurements within the Blunt Body Shock Layer in an Arc-Jet Flow", AIAA Paper No. 97-0990, Jan., 1997; also *J. Thermophysics and Heat Transfer*, **12**, pp. 190-197, (1998).
66. C. S. Park, M. E. Newfield, D. G. Fletcher, and T. Gökçen "Spectroscopic Measurements of the Flows in an Arc-Jet Facility", AIAA Paper No. 98-0893, 36th Aerospace Sciences Meeting; also *J. Thermophysics and Heat Transfer*, **13**, pp.60-67, (1999).
67. T. Gökçen, "Computation of Nonequilibrium Viscous Flows in Arc-Jet Wind Tunnel Nozzles", AIAA Paper No. 94-0254, 32nd Aerospace Sciences Meeting, (1994).
68. T. Gökçen, "Effects of Freestream Nonequilibrium on Convective Heat Transfer to a Blunt Body", *J. Thermophysics and Heat Transfer*, **10**, April-June, pp.234-241, (1999).
69. E. E. Whiting, J. O. Arnold, and G. C. Lyle, "A Computer Program for a Line-by-Line Calculation of Spectra from Diatomic Molecules and Atoms Assuming a Voigt Line Profile", NASA TN D-5088, March, (1969).
70. E. Venkatapathy, J. W. Naughton, and D. G. Fletcher, "Experimental and Computational Study of Sonic and Supersonic Plumes", AIAA Paper No. 95-3496, AIAA Atmospheric Flight Mechanics Conference, August, (1995).
71. C. S. Park, D. G. Fletcher, and J. M. Donohue, "Spatially Resolved Shock Layer Emission Measurements and Analysis in an Arc-Jet Facility", AIAA Paper No. 99-1046, 37th Aerospace Sciences Meeting, Jan., (1999).
72. U. B. Mehta, "Guide to Credible Computer Simulation of Fluid Flows", *J. Propulsion and Power*, **12**, pp. 940-948, (1996).